THE PENNSYLVANIA STATE UNIVERSITY
SCHREYER HONORS COLLEGE

DEPARTMENTS OF ENGINEERING SCIENCE AND MECHANICS AND
MECHANICAL AND NUCLEAR ENGINEERING

MULTI-FIELD ACTUATION OF POLYMER BASED STRUCTURES

SARAH MASTERS
Spring 2016

A thesis
submitted in partial fulfillment
of the requirements
for a baccalaureate degree
in Engineering Science
with interdisciplinary honors in Engineering Science and Mechanical Engineering

Reviewed and approved* by the following:

Zoubeida Ounaies
Professor of Mechanical Engineering
Thesis Supervisor
Honors Adviser

Clifford Lissenden
Professor of Engineering Science and Mechanics
Honors Adviser

Mary Frecker
Professor of Mechanical Engineering
Faculty Reader

Judith A. Todd
P.B. Breneman Department Head Chair
Professor, Department of Engineering Science and Mechanics

* Signatures are on file in the Schreyer Honors College and Engineering Science and Mechanics Office.

ABSTRACT

In this project, active materials and sample configurations were explored with the goal of creating multi-field actuators, i.e., materials that respond to multiple stimuli to deform and change shape. Specifically, PVDF-TrFE- CTFE (terpolymer) and PDMS with barium ferrite particles were the two types of active materials used. Terpolymer is an electroactive polymer material, which actuates when an electric field is applied, and the PDMS with barium ferrite particles is a magnetoactive material, which actuates when placed in a magnetic field. By building different actuator configurations using these active materials, deformation and shape change can be achieved using both electric and magnetic fields. The main two motions observed throughout this project were bending (curvature across the entire sample) and folding (localized curvature at a notch). First, bending in a unimorph was explored; the unimorph was fabricated using solution cast terpolymer as the active material with scotch tape added to the sample as the inactive material. When an electric field is applied to this type of sample, the nanodomains present in the terpolymer cause it to contract in the thickness and expand in the length of the sample. Attaching a layer of scotch tape (inactive substrate) to the terpolymer restricts the planar expansion of the terpolymer when electric field is applied. This configuration, referred to as a unimorph, results in a bending motion towards the inactive substrate under electric field. Next, notches are introduced in the unimorph to transform the bending into folding; specifically, two smaller pieces of scotch tape were added on to the single layer of tape that was first placed on the terpolymer. A gap, i.e., notch, is left in between the two smaller pieces of tape that are added to the top of the sample. In the notched area, since there is less inactive substrate, these areas will exhibit more localized bending than the rest of the samples. Both single notch and double notch folding were explored. Double notch samples showed greater actuation, to the point where the sample curled up on itself because a large amount of folding was produced in both notches. Next, PDMS with barium ferrite

particles was used to create a unimorph bender that would actuate when a magnetic field was applied. The barium ferrite particles are permanent magnetic particles, so when they are added to the PDMS and the entire sample is cured under a magnetic field, the resulting material has a magnetic pole direction. When the sample is then placed in an applied magnetic field, the sample actuates (bends) to try to align the poled direction of the sample with the direction of the external magnetic field. Finally, terpolymer and PDMS with barium ferrite particles were combined (attached together using an adhesive spray) into a bimorph structure. Both bending and folding actuators were investigated using this bimorph configuration. These multi-field actuators respond to both electric and magnetic fields. In conclusion, multi-field actuation of a single bimorph sample was achieved using both an electric and magnetic field. Both multi-field bending and folding were successfully demonstrated and quantified.

TABLE OF CONTENTS

LIST OF FIGURES

LIST OF TABLES

ACKNOWLEDGEMENTS

I would like to thank Dr. Zoubeida Ounaies, my research advisor, for allowing me to work on this project and for all of the support throughout my research. By working under Dr. Ounaies, I have been able to see research done at its best, and have learned so much that I will carry with me to my future endeavors. Thank you for being a great role model and for all of the help throughout this project. I would also like to thank Saad Ahmed for being my graduate mentor and for all of the help he gave me in the lab. Thank you to everyone in the EMCLab for welcoming me into the group and for the continued support throughout this project. I would also like to thank Dr. Mary Frecker and Dr. Paris von Lockette for all of the help and suggestions given during our weekly group meetings as well as any time I needed clarification on something. Also, I would like to thank everyone involved with the EFRI project for all of the help and support and welcoming environment that made working on this project very enjoyable. Specifically, I would like to thank Erika Arrojado, Shreya Trivedi, and Corey Breznack for the help I received in the lab.

I would like to extend my gratitude to the Engineering Science department for providing me with a great education and great department to be in. I would like to thank Dr. Clifford Lissenden, my academic advisor, for all of the help given to me throughout my entire four years here at Penn State.

Next, I would like to thank my siblings for all of the support and motivation you gave me. Finally, thank you to my parents who were always there to help me keep moving forward and for the endless amount of support and love you have given me. You have helped me realize that with hard work and dedication, there is no problem I cannot tackle.

I would like to gratefully acknowledge the support of the National Science Foundation, grant number EFRI 1240459, and the Air Force Office of Scientific Research.

Chapter 1

Background and Problem Statement

This project is focused on a materials development study exploring the response of active polymers to multiple applied fields, specifically electric and magnetic fields. The geometry and configuration of the polymer-based materials are also explored with the goal of differentiating between bending and folding during the active response to external fields.

Origami Background and Motivation

Origami is an ancient art form where different shapes and objects are created by folding a single piece of paper [**1**]. This art form originated in Japan and the term origami came from the Japanese words *ori* and *kami*, which mean "folded" and "paper" respectively [**2**]. Although origami started as an art form, eventually some people saw origami as a technical challenge and began exploring how to create more complex structures [**2**]. People started analyzing the math needed to model origami structures as well as define different types of motion possible through origami [**1**] [**3**]. Recently, the field of origami engineering has emerged where people are looking into origami inspired designs to create structures that can fold from a flat sheet into complex 3D shapes. Origami engineering is an expanding field and has many promising future applications such as 'self-deployable origami stent grafts' for medical use [**4**], or a 'deployable solar array for space applications' [**5**]. One specific area being investigated is to apply active materials to origami structures instead of just using paper in order to complete the folding steps without manual manipulation [**3**]. Active materials are materials that respond to external stimuli such as heat or light to produce a mechanical response. Some active materials that are being investigated

for origami engineering include shape memory polymers [**6**], polymers that respond to optical stimuli [**7**], dielectric elastomers [**8**], magnetoactive elastomers [**8**], and relaxor ferroelectric terpolymers [**9**]. When using active materials with origami inspired structures, it is important to be able to describe the motion of the structure in a consistent way. The active material is usually connected to a substrate creating a unimorph sample. As a result, the substrate (if it is passive) constricts the motion of the active material leading to actuation that has been proposed as bending or folding [**8**]. Bending has a radius of curvature throughout the entire sample, whereas folding has a local crease or sharp edge that is created [**8**]. Throughout this project, the difference between bending and folding is further explored as well as different sample configurations in order to obtain both bending and folding.

Electrically Actuated Polymer

Some active materials exhibit coupling between electrical and mechanical response. A subclass of materials with electromechanical coupling is ferroelectric materials. Ferroelectric materials have a polarization that can be re-oriented by applying an electric field to the material [**10**]. Regions throughout the material that have uniform polarization are called ferroelectric domains [**10**]. These polarized domains cause the material to exhibit a remnant polarization, or the charge density or electric displacement (D) value when there is no electric field applied. As an electric field is applied, the electric displacement changes as seen in Figure 1 [**11**]. The relationship between the electric field and the electric displacement can be described as a hysteresis loop. By adding in defects such as chlorotrifluoroethylene (CTFE) to a ferroelectric material, a relaxor ferroelectric material, with mobile nanodomains, can be produced. By having nanodomains, rather than microdomains as in regular ferroelectric materials, the domains in

relaxor ferroelectric material can align and move more easily. Also, relaxor ferroelectric materials have a lower remnant polarization as seen in Figure 1 [**11**].

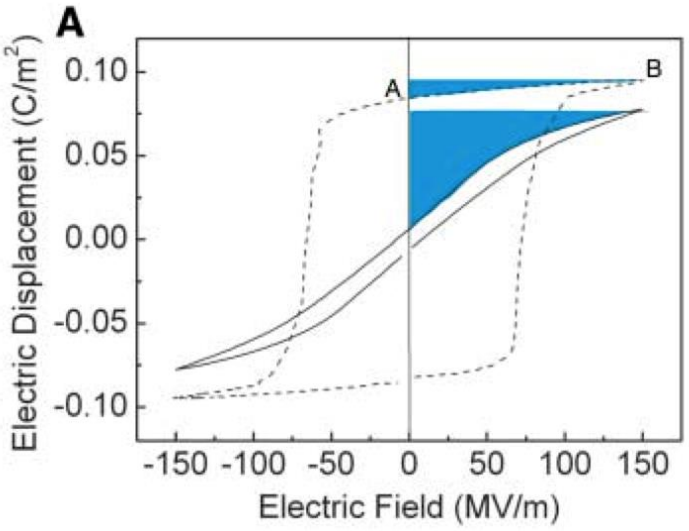

Figure 1: This figure shows the graph of electric displacement vs. electric field for the ferroelectric PVDF (the dotted line) and the relaxor ferroelectric PVDF (the solid line). The shaded in region represents the energy density [12**].**

Poly(vinylidene fluoride) PVDF was one of the first polymers to be considered a "ferroelectic polymer" [**13**]. Later, copolymers such as PVDF-TrFE were explored. Within PVDF-TrFE, there are two main phases, a ferroelectric phase and a paraelectric phase [**11**]. Some of the properties of the ferroelectric material can be enhanced near this phase change region, and by adding in defects, such as chlorotrifluoroethylene (CTFE), the PVDF-TrFE will become a relaxor ferroelectric material. In PVDF-TrFE- CTFE relaxor ferroelectric, the ferroelectric transition will be broader than in the regular ferroelectric and the ferroelectric-paraelectric transition temperature will be lower, improving some of the material's mechanical responses. In the normal ferroelectric phase, most of the polymer chains are in the all-trans conformation, which is polar, causing the material to start out with a non-zero charge density (D) when the electric field equals zero [**12**]. Once the defects are added to create a relaxor ferroelectric, most of

the chains are forced to transition to the TG and T_3G conformations, which are antipolar, causing a remnant polarization near zero as discussed previously [**11**] [**12**]. Figure 2 shows the three different conformations [**11**] [**14**] [**15**].

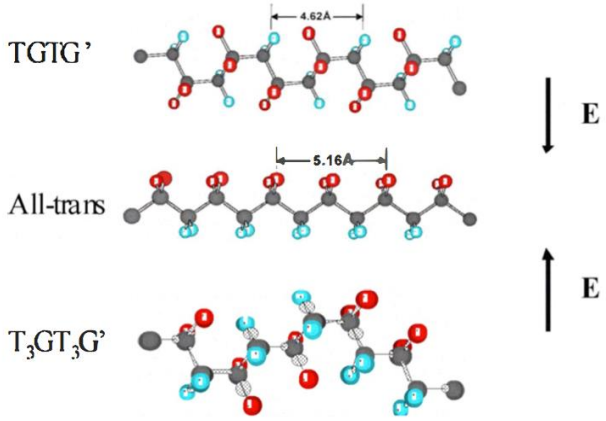

Figure 2: This figure lays out the three different types of conformations, TGTG' or T3G, TG, and All-trans [11**] [**14**] [**15**].**

For the purpose of an electrically active material, it is important for the polymer to have a high energy density. The energy density (U_e) refers to the amount of energy the material can store and can be defined as seen in

$$U_e = \int E\, dD \qquad \text{Equation 1}$$

. In this equation, E is the electric field and D is the electric displacement or charge density [**12**]. The energy density can also be seen as the blue shaded regions in Figure 1.

$$U_e = \int E\, dD \qquad \text{Equation 1}$$

One factor that affects the energy density of a dielectric polymer is the remnant polarization, or the D value when the electric field is equal to zero. In order to obtain a larger change in D, it is ideal to have the remnant polarization as close to zero as possible [**12**]. It can been seen in Figure

1 that the relaxor ferroelectric material has a remnant polarization close to zero, allowing for a larger change in D with the applied electric field than that of the regular ferroelectric material. This larger change in D produces a higher energy density.

Along with a high energy density, it is important for the polymer to have high electrostrictive strain for actuation purposes. Normal ferroelectric materials have relatively low strain levels (~0.1%) [**11**]. Near instability region like the ferroelectric-paraelectric transitions, strain levels can be enhanced as discussed before. When an electric field is applied to PVDF-TrFE- CTFE, the chains make a transition from the TG and T_3G conformations to the all-trans conformation. It is proposed that the change from the disordered TG and T_3G to the all-trans is what produces a big electrostrictive strain [**11**]. So, by applying an electric field to PVDF-TrFE-CTFE, which will be referred to as terpolymer in subsequent sections, the material contracts in the thickness and expands in the plane resulting in electrostrictive strain. This electromechanical strain response is a nonlinear function of the applied electric field. By attaching this material to an inactive substrate, actuation of the sample through bending or folding will occur. As the active material expands in the plane, the motion will be restricted by the inactive substrate since the substrate will not expand. Since the two materials are attached, this difference in expansion will lead to bending or folding of the sample depending on the configuration.

Magnetoactive Elastomer

Another type of active material used throughout this project is magnetoactive elastomers. Magnetoactive elastomers respond to an applied magnetic field to produce a mechanical response. Specifically, for this project, magnetoactive elastomers were created using barium hexaferrite particles. The barium hexaferrite used has a chemical composition of $BaFe_{12}O_{19}$ and is also known as M-type barium hexaferrite [**16**]. The barium hexaferrite particles are usually

formed as thin plates that are hexagonal in shape and have a large crystalline anisotropy direction perpendicular to the plate [**17**]. The magnetic easy axis (favorable direction of spontaneous magnetization) aligns with this crystalline anisotropy, so it aligns with the c-axis, which is perpendicular to the plate [**18**]. Previous studies have been done using barium hexaferrite as the additive permanent magnetic particles in an elastomer, and good actuation was achieved from the bender samples tested [**19**]. Another study has explored using elastomers with barium hexaferrite particles as the driving mechanism for locomotion by adding patches of the elastomers with the added particles to an inactive substrate [**20**]. A different study was conducted adding barium ferrite fibers to PVDF in order to create composite films [**21**]. These composite films exhibited a hard magnetic characteristic [**21**].

Barium hexaferrite particles are hard magnetic particles and were added to a PDMS substrate. After the addition of the barium hexaferrite particles, the samples were poled using magnets while curing. This aligned the magnetic axes (axes perpendicular to the plates) of the barium ferrite particles within the sample, giving the PDMS with barium ferrite particles added a remnant magnetization, or poled direction [**22**]. Once the material is cured, the barium ferrite particles can no longer move within the PDMS substrate, so below a magnetic field threshold, this poled direction is permanent. When an outside magnetic field is applied to the sample, after it has been poled and cured, a magnetic torque is created that tries to align the poled direction in the sample with the applied magnetic field direction as seen in Figure 3 [**23**]. This alignment will cause the sample to move, bend, or fold and is what will be referred to as magnetic actuation of the sample. By varying the ratio of barium ferrite particles to PDMS, samples can be created that will actuate at different amounts (different tip displacements or angles of folding) when the same magnetic field is applied. Varying the strength of the applied magnetic field will also change the amount the sample actuates (different tip displacements or angles of folding).

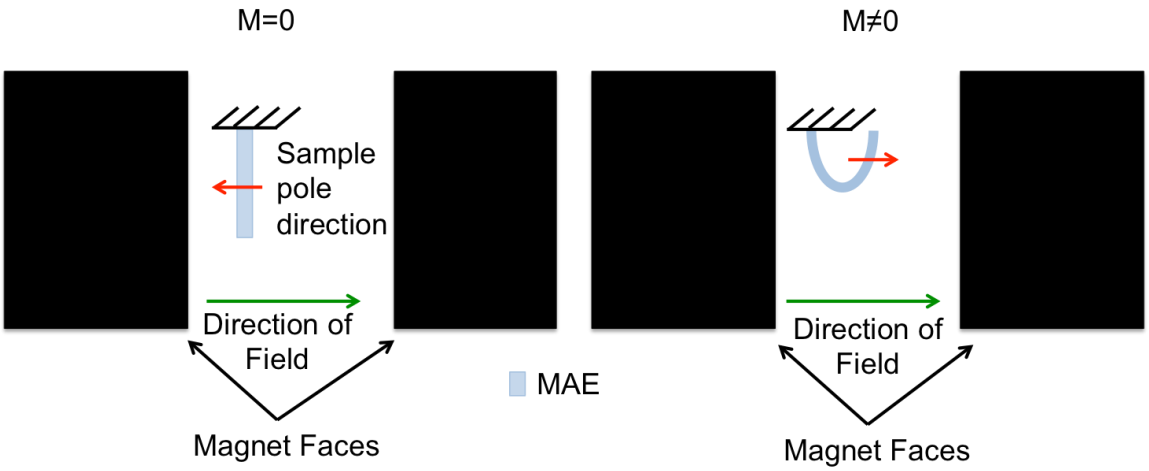

Figure 3: MAE actuation schematic

Multi-field Actuation

By incorporating two different types of active materials into one sample, multi-field actuation can be achieved. Some studies have been previously conducted looking into multi-field actuation with both electric and magnetic fields [**8**] [**21**]. Specifically, one study explored both a dielectric elastomer (DE), which would actuate when an electric field was applied, and a magnetoactive elastomer, which would actuate when a magnetic field was applied [**8**]. Throughout this study, each material was analyzed individually and then a multi-field simulation was presented at the end of the work [**8**]. A different group looked into fabricating one material that would respond to multiple fields, rather than just combining two active materials into one sample. This group explored adding barium ferrite fibers to PVDF to create composite films [**21**]. The resulting films did have hard magnetic characteristics, so the material in theory would actuate in response to an applied magnetic field [**21**]. Throughout this project, combinations of electroactive material (terpolymer) and magnetoactive material (PDMS with barium ferrite particles) are investigated. The main concept behind multi-field actuation is to produce different movement of the sample depending on what field is applied. Throughout this project, multi-field

actuation is achieved by making the sample bend or fold in one direction when an electric field is applied and bend or fold in the opposite direction when a magnetic field is applied as seen in Figure 4.

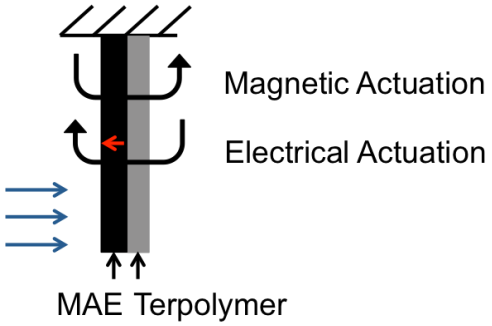

Figure 4: This schematic shows a multi-field sample that will actuate to the left when an electric field is applied and to the right when a magnetic field is applied.

Problem Statement

The goal of this research is to produce a multi-field actuation configuration that will respond to both electric and magnetic fields. This will be accomplished by exploring both electroactive material, terpolymer, and magnetoactive material, PDMS with barium ferrite particles. Each material will be explored individually and then combined into multi-field structures. One multi-field structure will consist of a strip of PDMS with barium ferrite particles attached to a strip of terpolymer which will create a multi-field bending actuator. The second structure will consist of two patches of PDMS with barium ferrite particles attached to a strip of terpolymer with scotch tape on it. This will create a multi-field folding actuator. To accomplish these multi-field actuator goals, first unimorph bending samples will be constructed and tested using each active material separately. Then, unimorph folding samples with one and two notches will be constructed and tested using terpolymer as the active material. Finally, the two materials will be combined into multi-field samples.

The next chapter, Chapter 2, will focus on the specific materials used, experimental set-ups, and measurement details. Chapter 3 will focus on the presentation, analysis, and discussion of experimental results. Chapter 4 will focus on the conclusions and future work.

Chapter 2 Experimental Procedure

Materials

The two main materials used in this project were P(VDF-TrFE-CTFE) (which will be referred to as terpolymer for the remainder of the thesis) and PDMS modified with barium ferrite particles (which will be referred to as MAE in the rest of the thesis). The terpolymer (P(VDF-TrFE-CTFE) with composition (61.8/30.4/7.8 mole %)) powder (Piezotech Arkema, France) was used throughout this project. Films of terpolymer were processed through solution casting; solution casting is a technique where the desired polymer solution begins as a liquid, so it can be easily spread (cast) into a thin sample and then cured to form the solid polymer. By using solution casting, relatively thin film thicknesses were achieved; specifically, thickness range is from 30 to 40 μm. Thinner samples are preferred because a higher electric field across the sample could be achieved with lower applied voltage, as seen in Equation 2, where E is the applied electric field, V is the applied voltage, and t is the film thickness.

$$E = \frac{V}{t} \qquad \text{Equation 2}$$

The terpolymer powder is dissolved in *N*,N- dimethylformamide (Sigma-Aldrich Chemistry, MO, USA) with a concentration of 12wt% [**9**]. The solution is mixed using a magnetic stirrer at 40° C for 2 hours. Then, it is degassed and cast onto a glass plate using a doctor blade. Next, the glass plate is placed in the oven at a 100° C for 2 hours under vacuum [**9**]. Once the terpolymer film is ready, it was post-processed by annealing it at 120° C for 9 hours under vacuum. These annealing conditions were used because previous studies have shown that

these conditions help produce higher crystallinity in the terpolymer, which leads to increased electrostrictive strain [**24**].

After the terpolymer is annealed, it is cut to size and sputtered with silver on both sides. Silver was sputtered to a thickness of 50nm using a Sputter Coater: Quorum EMS 150 RS (Electron Microscopy Sciences, PA, USA): first, a mask is laid over the surface of the film so that the electrode pattern does not cover the edges, leading to shorting and premature breakdown (see Figure 5). Two strips of copper wire tape were then added to the sample, one on each side, so that the positive and negative terminals from the power source could be attached to the electrodes (see Figure 5). The last step in fabricating the terpolymer actuator samples was adding an inactive substrate to the terpolymer to form a unimorph. Scotch tape is added as the inactive substrate by sticking the adhesive side of the tape to the terpolymer (see Figure 6a). Configurations for the bending and folding (notched) samples are shown in Figure 6.

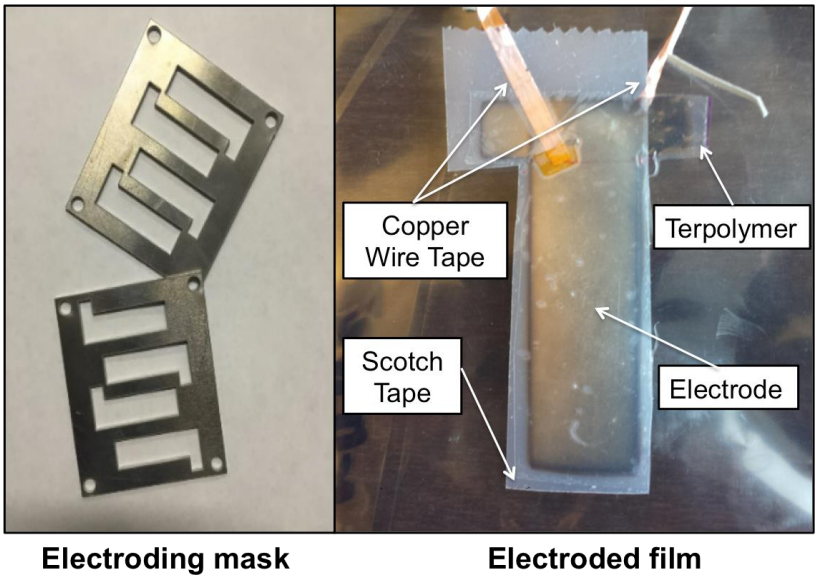

Figure 5: The electroding masks that keeps the silver electrode from covering the edges of the terpolymer sample (on the left) and terpolymer film after silver is sputtered on each side and scotch tape and copper wires are attached (on the right).

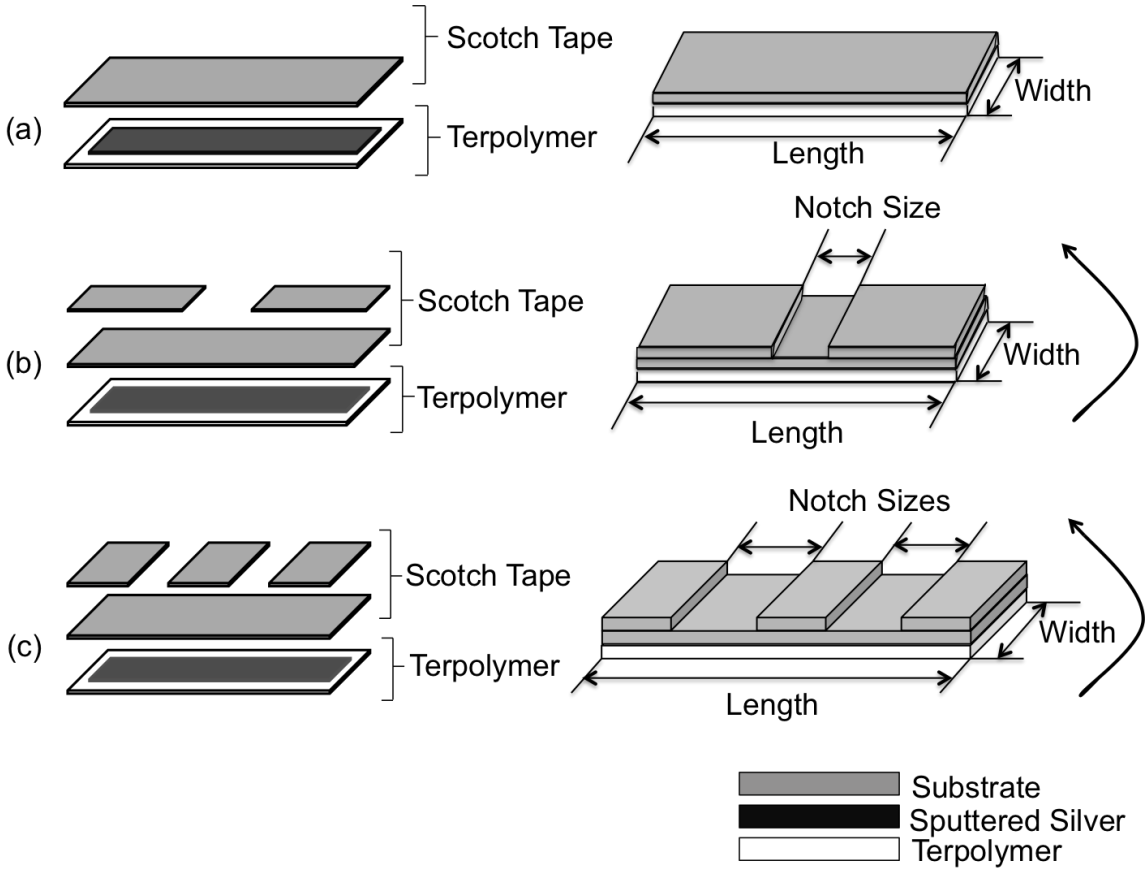

Figure 6: Bending and folding configurations for terpolymer actuator samples. (a) Bending (b) Single notch (c) Double notch

As seen in Figure 6, the folding sample configurations are more complex than the bending configuration. The general principle behind folding is to create an area on the sample where there is less inactive substrate, also referred to as a notch, which will cause the sample to show localized bending within this area when actuated. This localized bending will cause the overall sample to produce a folding motion. The notches were produced by adding extra small patches of scotch tape to the one complete layer of scotch tape that is first placed on the terpolymer, as seen in Figure 6b and 6c. The base layer of scotch tape is needed in order to produce the localized bending within the notch. If just the patches of tape were added without the complete first layer, then the terpolymer within the notched area would not be attached to any inactive substrate, so bending would not occur since the bending is produced by the difference in strain between the

terpolymer and the inactive substrate when the electric field is applied. These samples, referred to as folder samples, were produced with a single notch (as seen in Figure 6b) or two notches (double notch) (as seen in Figure 6c).

To fabricate the MAEs, barium ferrite particles (ESPI Metals, Oregon, USA, stock number: Knc6220) were added to PDMS (Sylgard 184 silicone elastomer kit was supplied by Dow Corning, MI, USA). In the beginning, the PDMS is a liquid, so in order to create solid samples from it, a curing agent (Sylgard 184 silicone elastomer curing agent, Dow Corning, MI, USA) must be mixed with the liquid PDMS (at a proportion of 1:10, curing agent:PDMS) and then the solution is cast onto a glass slide. After this, the cast solution is placed in the oven at 100° C for 40 min in order to cure the sample. Then, the temperature is turned down to 60° C and a vacuum is applied for 20 min. This process creates a solid sample of plane PDMS with thicknesses ranging from 0.3 to 0.5 mm. In order to make the PDMS magnetically responsive, barium ferrite (BF) particles are added. The barium ferrite particles are hexagonal in shape and about 3 μm in length along the long axis (as specified by the manufacturer).

The procedure for adding BF to PDMS is summarized in the schematic/flowchart of Figure 7. First, liquid PDMS was mixed with Heptane (Alfa Aesar, MA, USA) at a ratio of 10g PDMS to 1g Heptane. Heptane was added to the mixture to act as a solvent for better dispersion of the barium ferrite particles throughout the solution and to lower the viscosity of the solution so it can be cast thinner, resulting in films with thicknesses ranging from 0.2 to 0.5mm. Once the PDMS and heptane were fully mixed, the solution was placed in the mechanical stirrer at approximately 220 rpm. Then, the barium ferrite particles were added (30 wt% content of barium ferrite particles in the BF/PDMS). The PEG (Sigma-Aldrich Chemistry, MO, USA) was also added at this time (PEG was 1/5 of the barium ferrite particle weight). At that point, the bath sonicator (Ultrasonic Bath 2.8L, Model 15337409, Fisher Scientific, PA, USA) was turned on and the solution was mixed with the mechanical stirrer (RW20 digital, IKA, NC, USA) while in the

bath sonicator for approximately 2 hours in order to obtain better dispersion of the barium ferrite particles. After the two hours, the bath sonicator was turned off while the mechanical stirrer was left on. After another hour, the curing agent was added to the solution at a ratio of 10g PDMS to 1g curing agent and the solution was left to stir for another hour. By the end, the solution had been in the mechanical stirrer for approximately 4 hours total. Then, the solution was degassed to remove air bubbles and cast onto a glass plate. The plate was then placed in a magnetic field in an oven at 105° C for 2 hours in order to simultaneously cure and pole. By placing the solution in the magnetic field, the particles would align to that field and create a poled direction in the sample. Once the sample was fully cured, this poled direction would be permanent below an applied magnetic field threshold. This produced thin films of magnetoactive material that ranged in thickness from 0.2 to 0.5 mm and had a 7.70 volume % (30 wt%) barium ferrite particles to PDMS. Figure 8 shows an image of one of the final films. This fabrication process was developed because thinner samples of MAE material are needed to prepare multi-field samples. Thinner samples of MAE are beneficial for multi-field actuators in order to reduce the stiffness of the MAE and the weight of the sample, allowing the terpolymer to actuate (bend or fold) to a greater distance when an electric field is applied to the sample. The MAE material was then cut to the same size as the terpolymer samples to prepare unimorph and multi-field bending samples (1 cm x 3 cm) and cut into patches to prepare multi-field folding samples (1 cm x 1 cm). The configurations of the multi-field bender and folder samples can be seen in Figure 9. As mentioned before, the magnetoactive material was then added to the terpolymer by using Scotch super 77 multi-purpose adhesive spray.

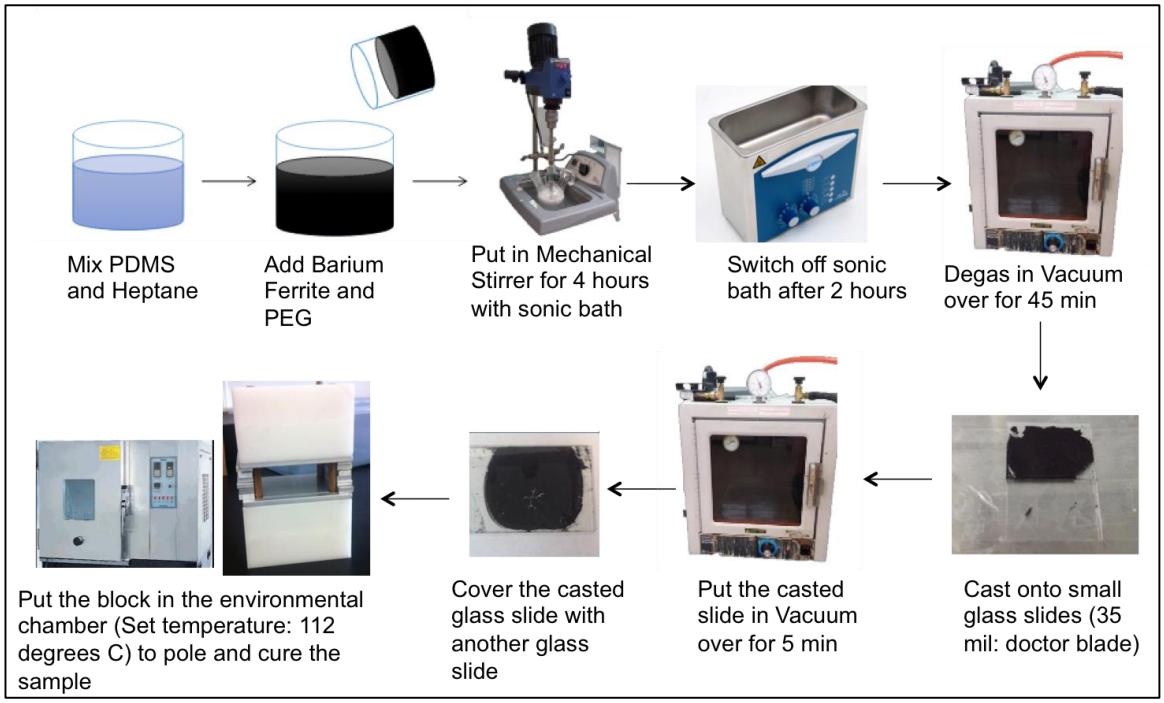

Figure 7: Summary flowchart of how to create a PDMS sample with barium ferrite particles added.[1]

Figure 8: Image of final film of PDMS with barium ferrite particles added. (Film is in between two glass slides)

[1] Thank you to my labmate Shreya Trivedi for providing the schematic for the flowchart on processing of a PDMS sample with barium ferrite particles.

For multi-field actuators, MAE strips were used as the inactive substrate. The MAE patches were adhered to the terpolymer using Scotch super 77 multi-purpose adhesive spray. Configurations for the bending and folding (notched) multi-field actuator samples are shown in Figure 9. Images of the actual samples can be seen in Figure 10.

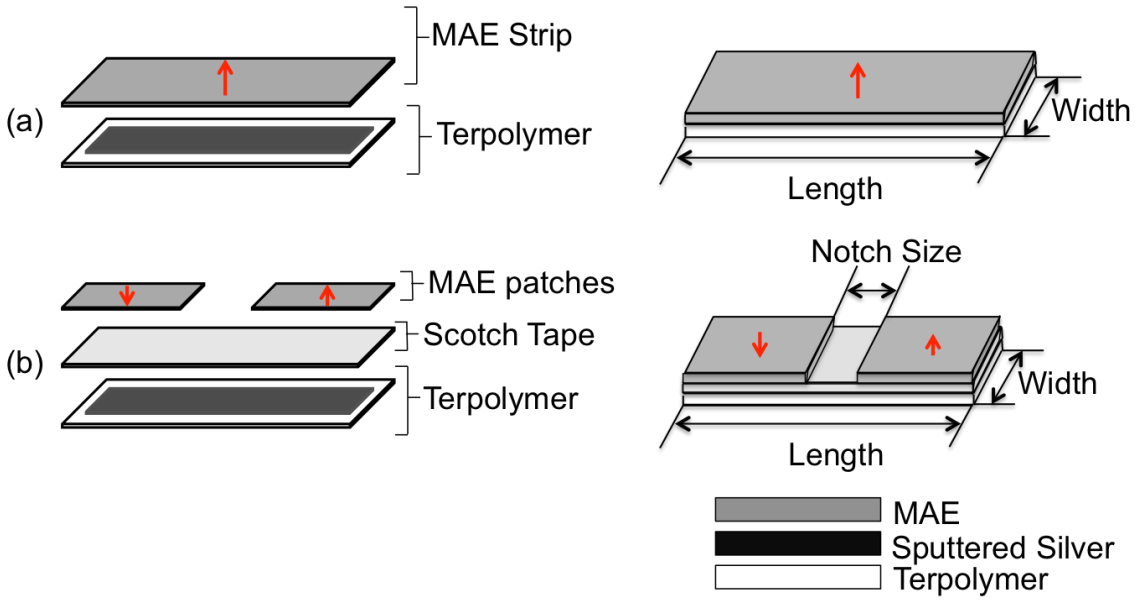

Figure 9: Bending and folding configurations for multi-field actuator samples. (a) Bending (b) Folding. Red arrows indicate poling direction of MAE.

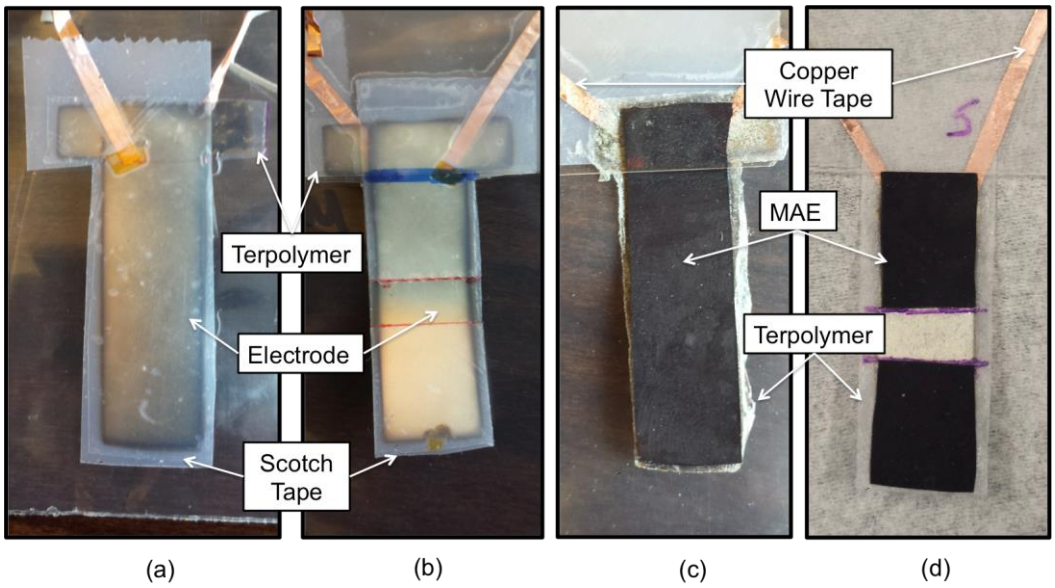

Figure 10: Images of electrical and multi-field actuator samples; (a) Terpolymer unimorph bender sample (b) Terpolymer unimorph folder sample (c) Multi-field bender sample and (d) Multi-field folder sample.

Magnetic and Electrical Characterization Experimental Setups

Two different setups are used for magnetic and electric characterization, one for applying the electric field to the sample and one for applying the magnetic field to the sample. When both fields were applied to the same sample, both setups were combined.

A photo of the overall electrical characterization setup is shown in Figure 11. The two instruments used for electrical actuation are the voltage amplifier and the function generator. In order to apply specific DC voltages to the sample, the function generator must be set to the High Z and DC modes. Then, the desired voltage is typed into the function generator and the voltage amplifier supplies the desired voltage to the sample. For the electrical actuation of the terpolymer unimorph samples, a DC voltage was applied to the sample in a range from 0 to 3 kV. This would produce an applied electric field between 0 and 90 MV/m, given that the thickness of the terpolymer was between 30 to 40 μm. The top of the sample was taped to a glass slide to produce

a cantilever as seen in Figure 12a. Then, the glass slide was held up with the sample hanging down so gravity was downward (again Figure 12a). Once the sample was held in place, the terminals from the voltage amplifier were connected to the copper wires from the sample. Then, different voltages were applied to the sample using the function generator. Videos from a camera on a tripod were taken throughout the entire actuation of each sample. In a later section (Actuation Measurement Details), a description of the video analysis and quantification of the electrical actuation will be detailed.

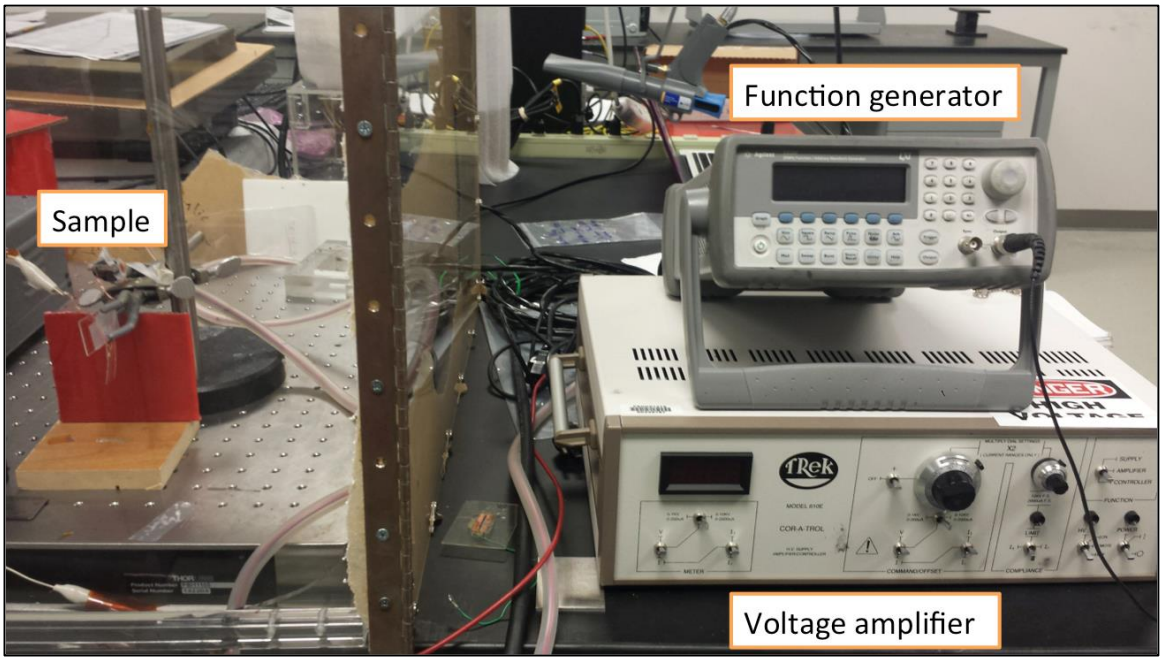

Figure 11: Electrical actuation setup.

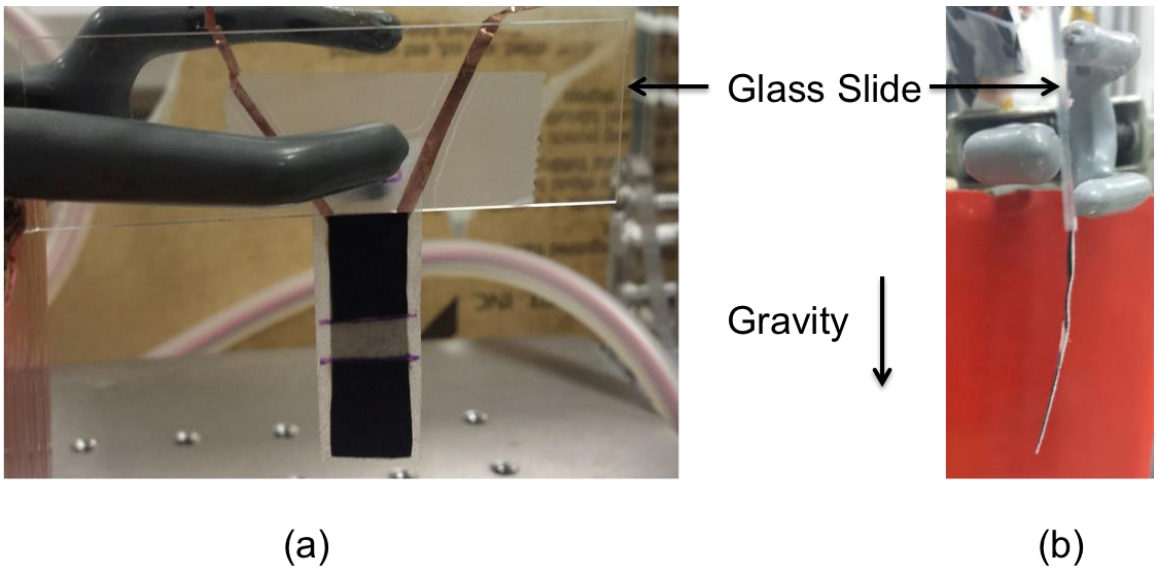

Figure 12: Sample attached to the glass slide to give the sample a cantilever constraint. (a) Front view, (b) Side view.

An image of the magnetic characterization setup is shown in Figure 13. Within Figure 13, the two instruments used for magnetic characterization, the C-magnet and power source, can be seen. The power source is connected to a C-shaped electromagnet (C-magnet) and by turning on and changing the current the power source is applying to the C-magnet, the magnetic field produced between the two faces of the magnet changes. The MAE sample was attached to a glass slide using tape to produce a cantilever configuration. The glass slide was then held in between the two faces of the C-magnet as seen in Figure 14. The C-magnet was in turn connected to the power source. The magnetic field was then varied by changing the amount of current the power source was supplying. A Gauss meter was used to correlate the current supplied to the magnetic field produced in the C-magnet as seen in Table 1. Videos form a camera on a tripod were taken throughout the entire actuation of each sample. In section Actuation Measurement Details, details on image analysis and quantification of magnetic actuation is given.

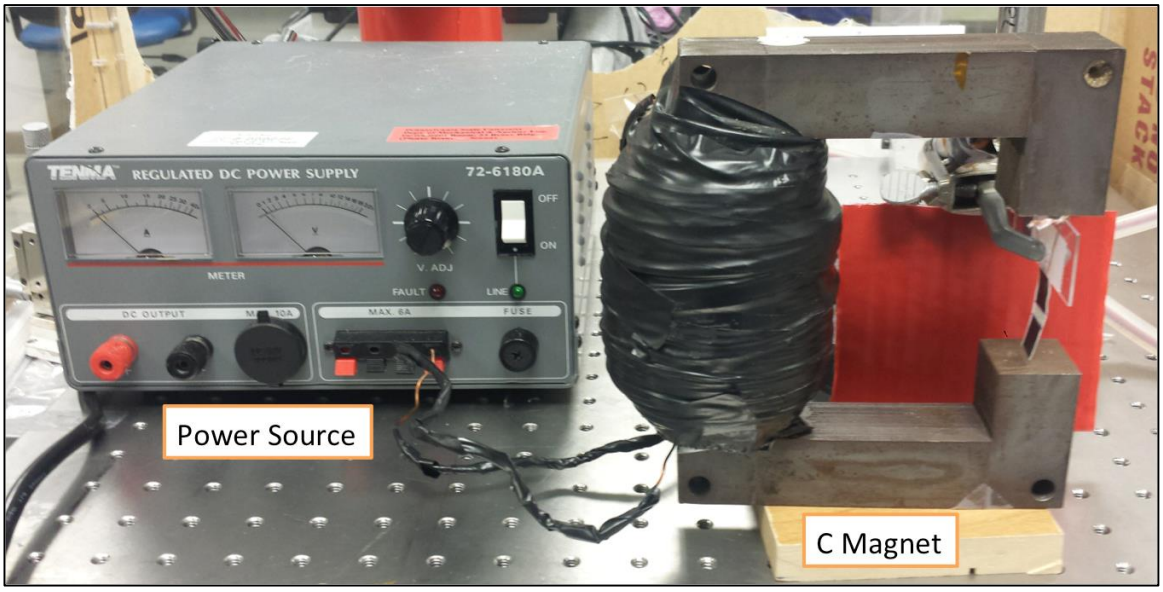

Figure 13: Magnetic actuation setup.

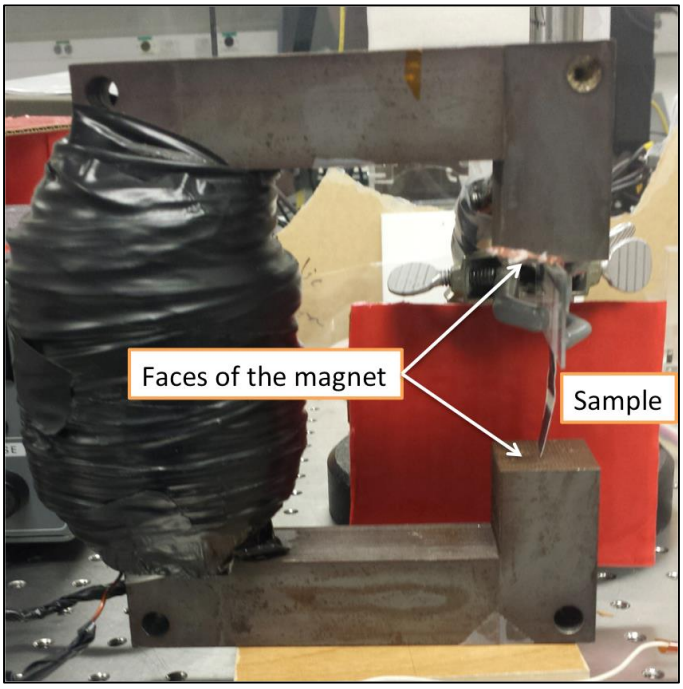

Figure 14: Sample within the C magnet.

Table 1: Magnetic Field Strength Calibration for the C-Magnet

Voltage (V)	Current (A)	Field Strength H (mT)
0	0	0.131
1	0.6	6.011
2	1.14	11.607
3	1.76	18.378
4	2.32	24.001
5	2.93	29.569
6	3.49	35.262
7	4.06	41.103
8	4.62	44.898
9	5.21	46.618
10	5.72	49.308
12	6.86	52.713
14	7.9	54.586
16	8.94	56.403
18	9.95	57.774
20	10.7	58.843
25	11.74	60.433
30	13.8	61.832

For the multi-field actuation, the electrical and magnetic actuation setups were combined. The sample was held inside the C-magnet while the copper wires from the terpolymer side of the sample were attached to the power source terminals for electrical actuation. Two different power sources were used, one connected to the C-magnet and the other connected to the sample. Figure 15 shows the combined setup. With this setup, both an electric field and a magnetic field could be applied to the sample without having to move the sample. This allowed for continuous actuation of the electric field and then the magnetic field or visa versa.

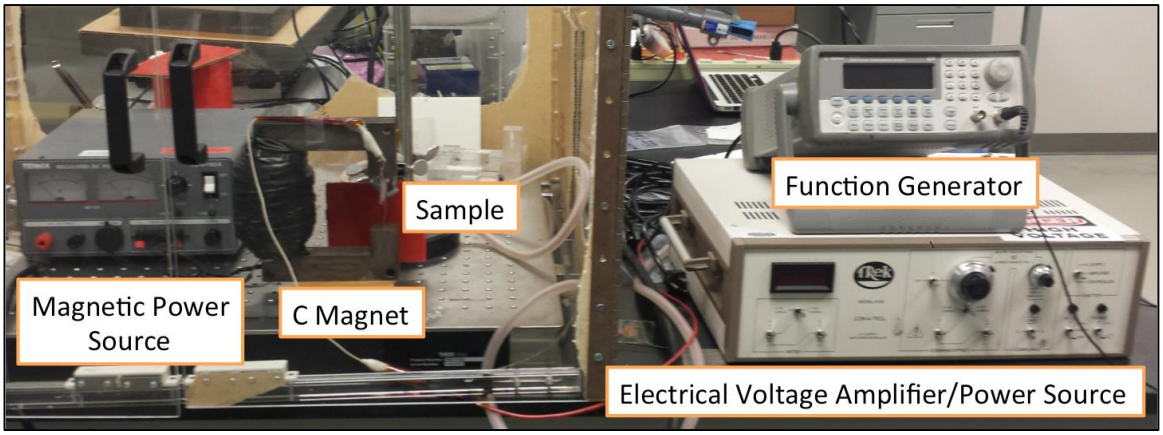

Figure 15: Multi-field actuation setup.

Larger magnets were later used to test the magnetic actuation of the multi-field samples because these magnets could produce a larger magnetic field than the C-magnet previously mentioned. The multi-field bender sample (see **Figure 10**) was tested in the horizontal magnet as shown in **Figure 16**. Not only did this magnet produce a higher field, it also allowed the sample pole direction to start at an angle of 180° from the applied field direction, unlike the C magnet where the pole direction of the sample started at an angle of 90° from the applied field direction (see **Figure 17**). This greater offset start angle allowed the sample to actuate more in order to align the sample pole direction with the applied field direction. A Gauss meter was used to correlate the current supplied to the magnetic field produced in the horizontal magnet as seen in **Table 2**.

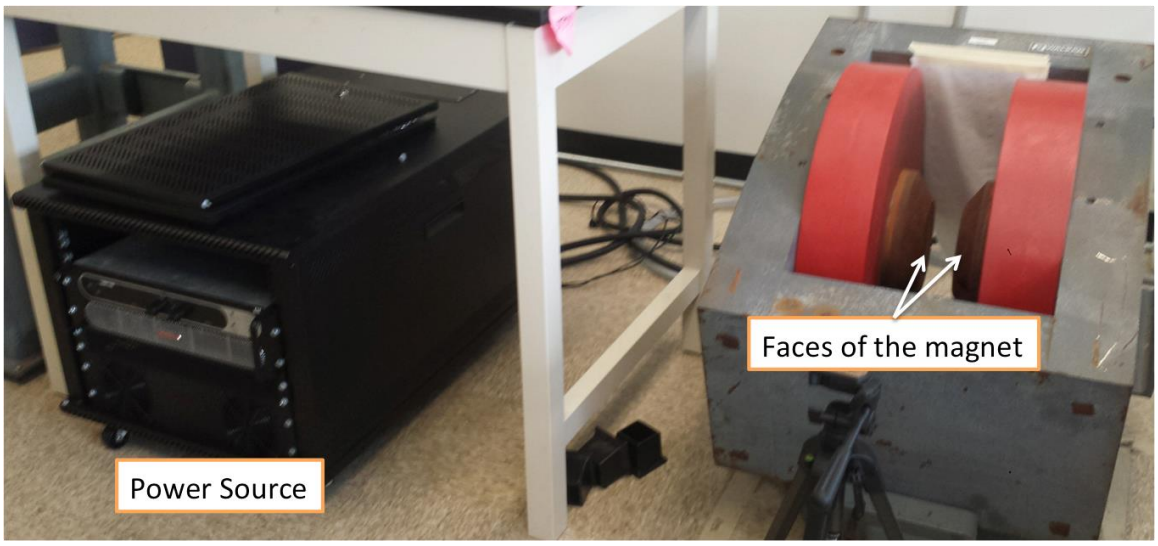

Figure 16: Horizontal magnet.

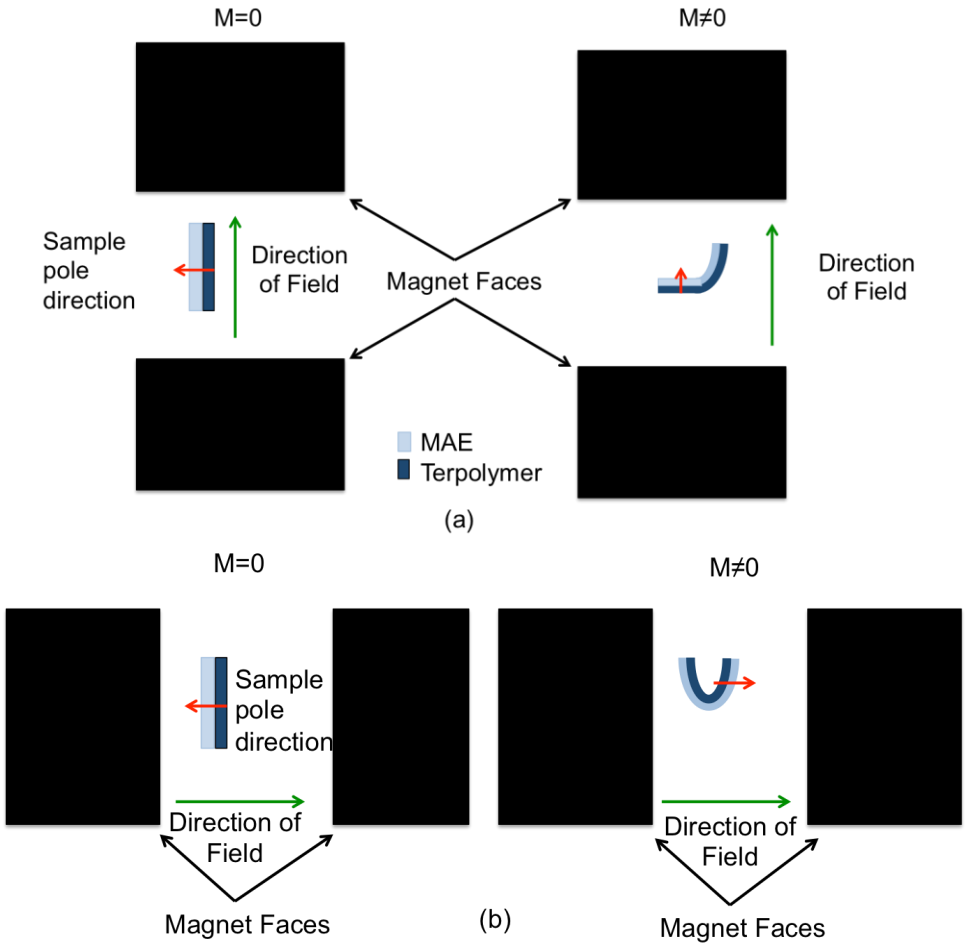

Figure 17: (a) Schematic of multi-field bender sample in the C-magnet with a 90° starting angle between the sample pole direction and direction of the field (b) Schematic of multi-field bender

sample in the horizontal magnet with a 180° starting angle between the sample pole direction and the direction of the field.

Table 2: Magnetic Field Strength Calibration for the Horizontal Magnet[2]

Voltage (V)	Field (mT)	Current (A)
0	2.48	0
2	34.5	1.1
4	62.3	2
6	94.8	3
8	134.2	4.3
10	164.1	5.3
12	197.7	6.5
14	225	7.6
16	247.8	8.7
18	279.2	9.8
20	307.5	10.9
22	338.9	12
24	369.5	13
26	400.5	14.2
28	431.2	15.2
30	461.4	16.4
32	489.2	17.5
34	521.2	18.6
36	550.4	19.7
38	580.6	20.7
40	612.4	21.8

The multi-field folding sample (see Figure 10) was tested in the vertical magnet as shown in Figure 18. This sample was tested in the vertical magnet rather than the horizontal magnet because this allowed each patch on the sample (the patches had opposite pole directions) to start with the pole direction at an angle of 90° to the applied field direction (as seen in Figure 19b). In the horizontal magnet, one patch would have started with a pole direction at an angle of 180° while the other patch would have started at an angle of 0° to the applied field (as seen in Figure 19a). In this case, only the one patch (the one starting at an angle of 180°) would contribute to the

[2] Thank you to my lab mate Corey Breznack for providing the calibration data.

actuation rather than both patches contributing to the actuation, which was seen using the vertical magnet. A Gauss meter was used to correlate the current supplied to the magnetic field produced in the horizontal magnet as seen in Table 3.

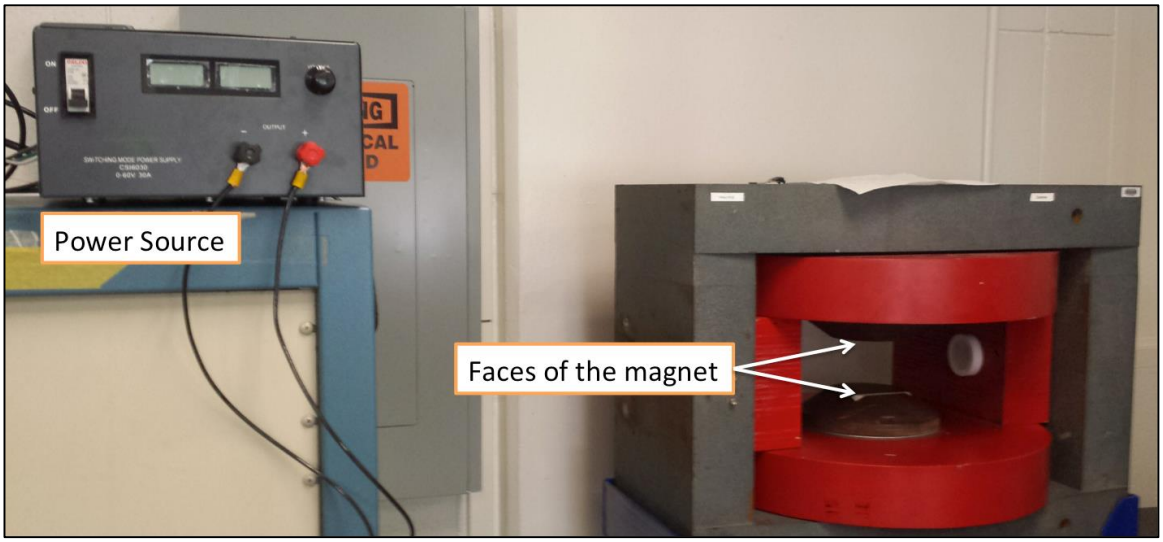

Figure 18: Vertical magnet.

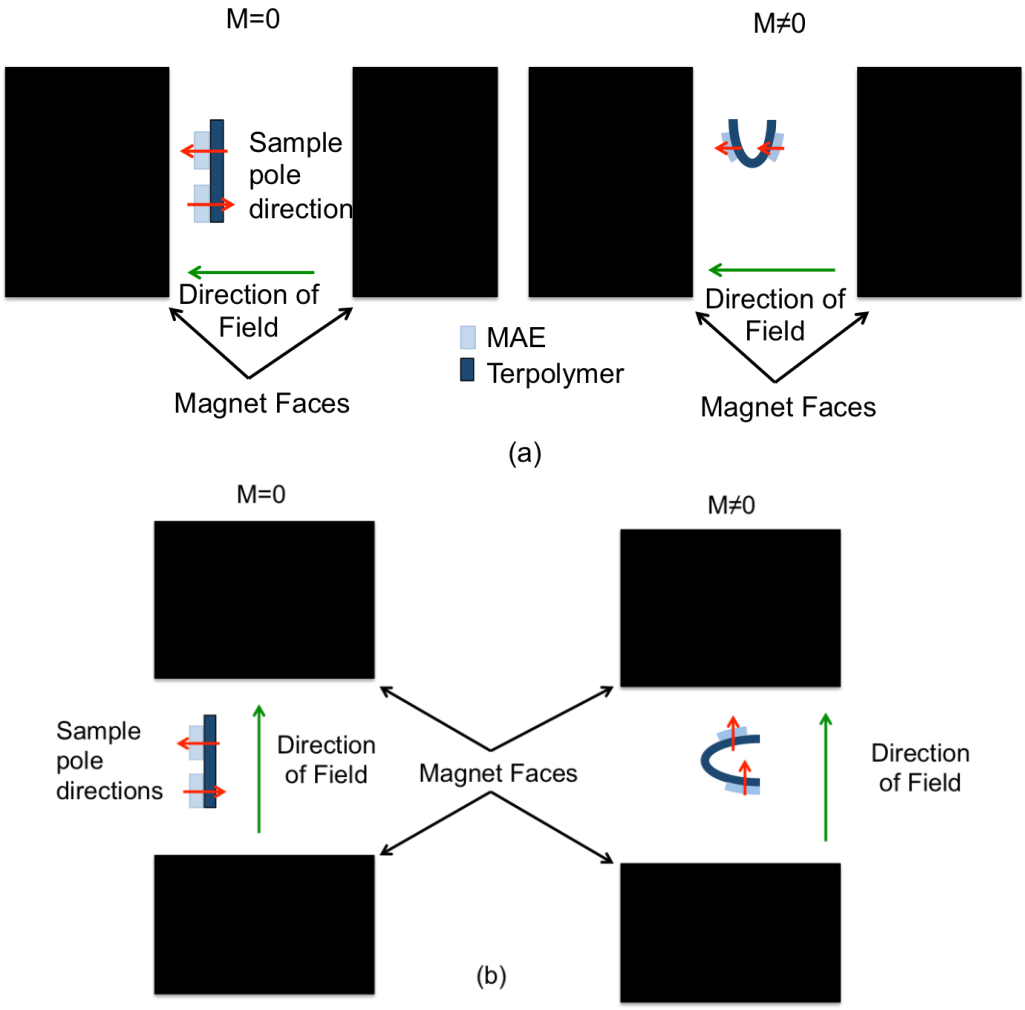

Figure 19: (a) Schematic of multi-field folder sample in the horizontal magnet where only one MAE patch is contributing to the actuation of the sample at fields where M≠0 (b) Schematic of multi-field folder sample in the vertical magnet where both MAE patches contribute to the actuation of the sample.

Table 3: Magnetic Field Strength Calibration for the Vertical Magnet[3]

Voltage (V)	Current (A)	Field (mT)
0	0	7.2
0.9	2	11.5
2	4	29.4
2.9	6	44.7
3.9	8	61.1

[3] Thank you to my lab mate Corey Breznack for providing the calibration data.

4.8	10	76.1
5.8	12	92.9
6.7	14	107.8
7.7	16	123.2
8.8	18	140.5
9.8	20	156.9
10.6	22	171.4
11.7	24	187.5
12.7	26	203.2
13.6	28	217.8
14.5	30	233.6

Actuation Measurement Details

Four main quantities were measured throughout these experiments; tip displacement, X and Y tip displacement, distance tip traveled, and angle. Depending on the type of experiment, one or more of these quantities were measured. For example, folding angle was measured for folding experiments but not bending experiments. As mentioned above, all experiments were video recorded. For the analysis of the experiment, still frames from the video were taken at each applied (electric or magnetic) fields and saved as images. Then measurements were taken using the imaging software ImageJ64. Using this software, the image at a specific applied field was overlaid with the image at zero applied field as seen in Figure 20.

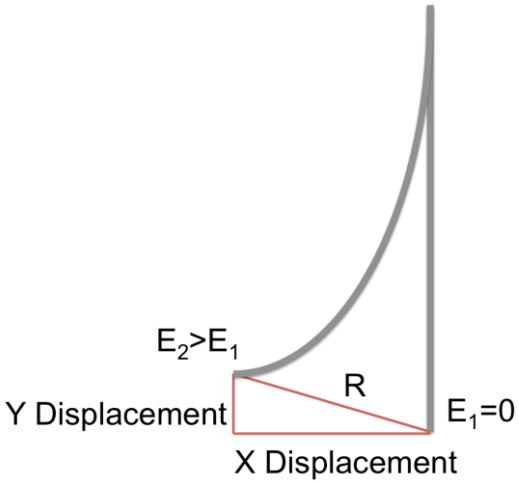

Figure 20: Overlay schematic of zero applied field and a non-zero applied field with measurement of tip displacement R, X displacement, and Y displacement.

Once the two pictures were overlaid with 50% transparency, the quantities discussed above could be measured. In ImageJ64, the length scale of the given image was calibrated by using the line function. Since the length of the sample was known, a line was drawn over the length of the sample and was assigned that value as seen in Figure 21. After the scale is set, distance measurements can be taken. Tip displacement was measured by drawing a line from the front edge tip of the sample at zero applied field to the front edge tip of the sample at an applied field as shown in Figure 20. The length of this line was then measured and recorded as the tip displacement at that applied field.

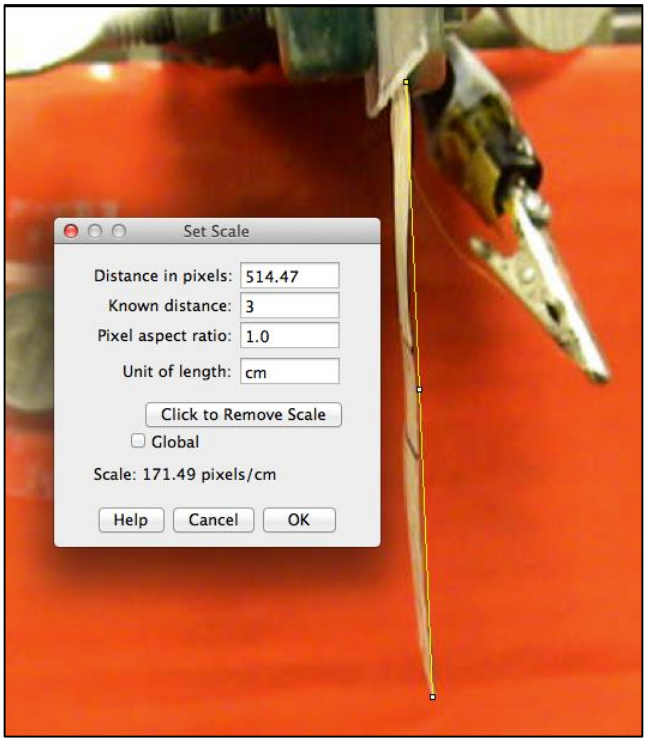

Figure 21: Image of the set scale function for a 3 cm sample.

For some experiments, the X and Y displacement of the tip were measured separately. This was done by placing a point at the front edge tip of the sample at zero applied field and at the front edge tip of the sample at an applied field. At each point, the X and Y coordinates were recorded. Then, to get the displacement, the difference between the X coordinates was recorded as the X displacement and the difference between the Y coordinates was recorded as the Y displacement (as seen in Figure 20).

Some samples curled on themselves, as seen in Figure 22. Because of this, measuring the tip displacement R does not appropriately capture the curling. Once the sample began to curl, the tip displacement appears to become smaller although the sample is actuating more, as seen in Figure 22. In this case, the distance that the tip traveled was calculated instead. The distance the tip of the sample traveled was measured by taking the difference between the tip location at a

given applied voltage and the previous location at the previous applied voltage. This difference was then added to the total distance traveled.

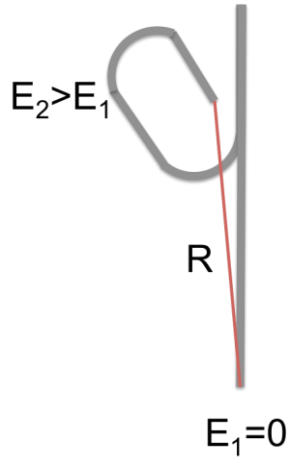

Figure 22: Schematic of a notched terpolymer sample actuated at a high electric field which causes the sample to curl or fold onto itself.

For notched folding samples (seen in Figure 6), the angle of the sample was measured at all the applied fields. Once the image at an applied field was overlaid on the image at zero applied field, the angle function in ImageJ64 was used to measure the angle between the original position of the sample and the position in the applied field as illustrated in Figure 23. Since some of the samples twisted during actuation, the angle was always taken from the front side edge of the sample and the line was drawn tangent to the tip of the sample. The tip displacement R was also measured from the overlaid images (as seen in Figure 23).

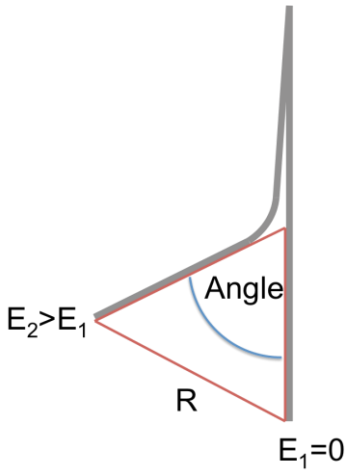

Figure 23: Measurement of the angle and tip displacement for a single notch terpolymer unimorph under an applied electric field (E_2).

For double notched samples (as seen in Figure 6), the angle created by both notches was measured and recorded at each applied electric field. First, the image of the sample at a given applied voltage was overlaid with the sample at zero applied voltage. Then, the angle function in ImageJ64 was used to measure the angle between the middle section of the sample at the applied voltage and the sample at zero applied voltage (angle 1). The angle between the tip of the sample at the applied voltage and the sample at zero applied voltage was also measured (angle 2). Both angle 1 and angle 2 and how to properly measure them can be seen in Figure 24. The tip displacement R was also measured for the overlaid images as seen in Figure 24.

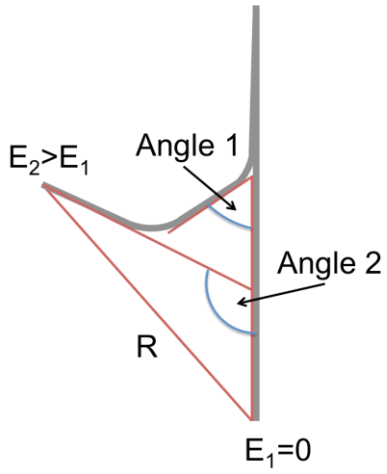

Figure 24: Measurement of angle 1, angle 2, and tip displacement R for a double notch terpolymer unimorph under an applied electric field (E_2).

Chapter 3 Results and Discussion

Bending Actuation

Bending was first explored by creating a unimorph using terpolymer as the active material. The bending configuration of the samples can be seen in Figure 6 (a). Different sample dimensions were tested, as seen in Table 4. As discussed in Chapter 2, still images were taken from the video at each applied electric field for each sample. A compilation of the images taken for bending sample 3 is shown in Figure 25. From these still images for each sample, the tip displacement, tip displacement in the X direction, and tip displacement in the Y direction were all measured and are displayed in Figure 26, Figure 27, and Figure 28.

Table 4: Terpolymer Bending Sample Dimensions

Sample Number	Length (cm)	Width (cm)	Thickness (μm)
1	6	2	40
2	3.5	1	40
3	3	1	37

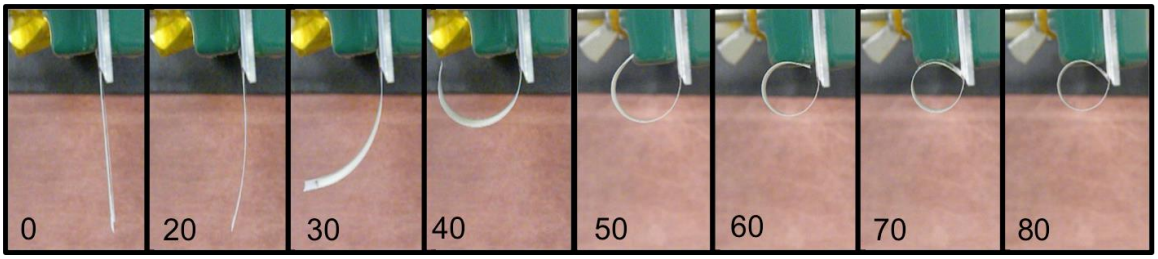

Figure 25: Terpolymer bending sample 3 actuation at different electric fields (0-80 MV/m).

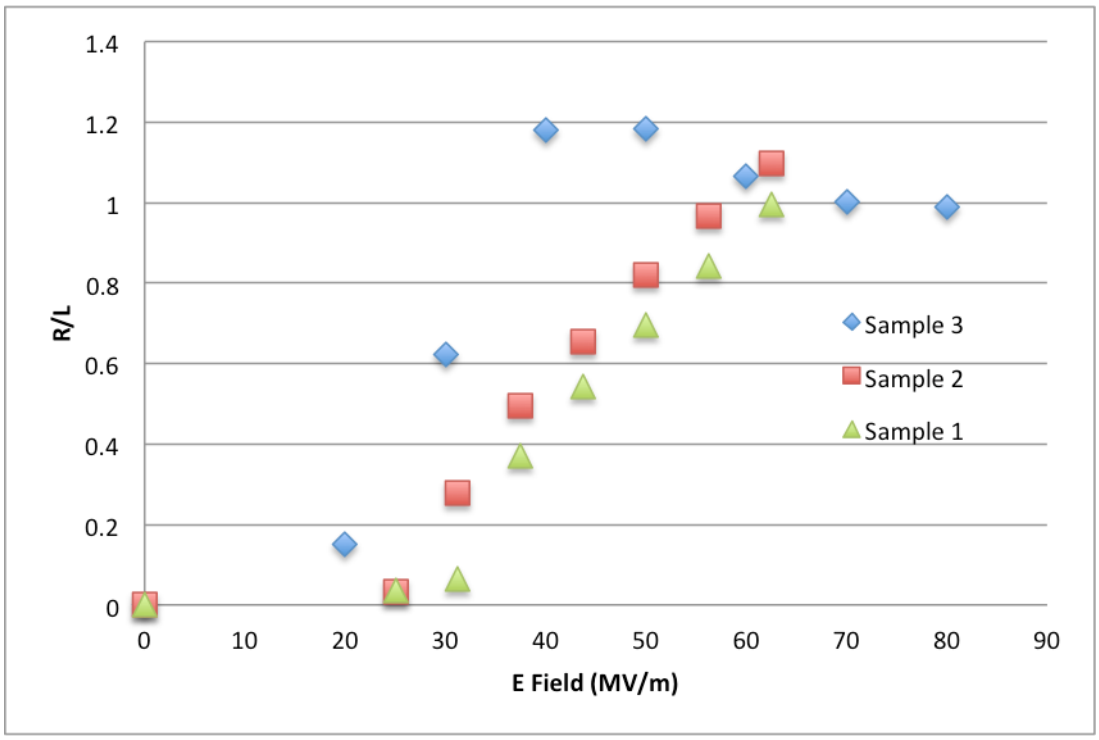

Figure 26: Normalized tip displacement for terpolymer bending unimorph.

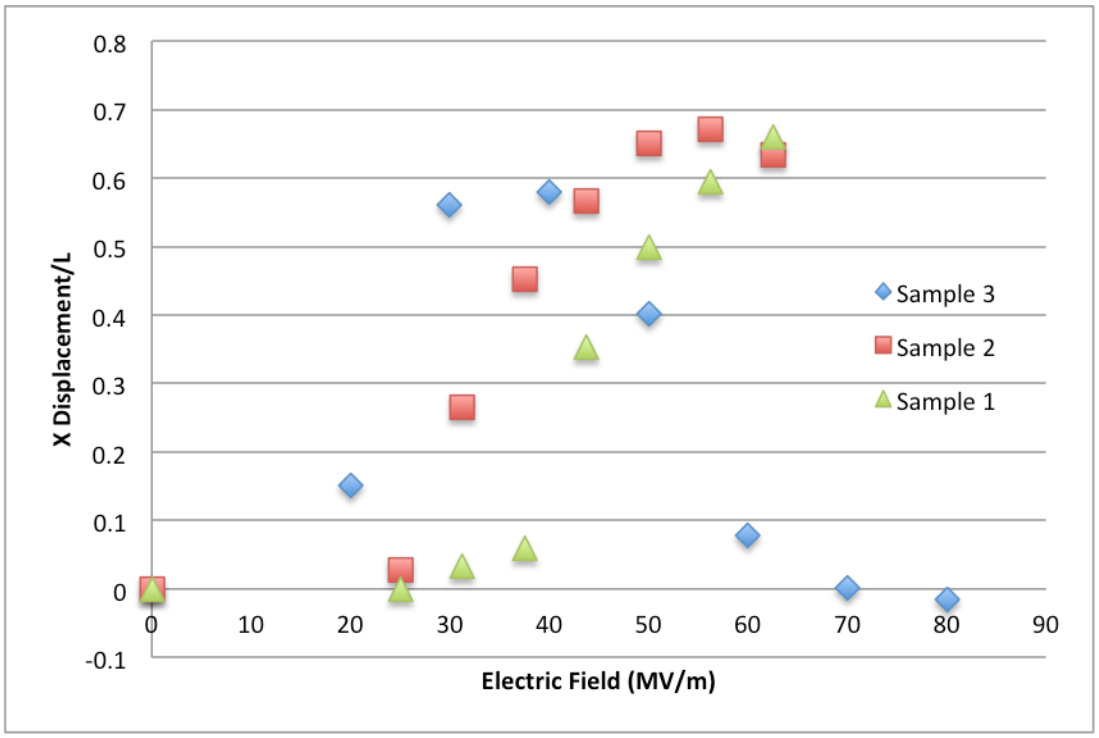

Figure 27: Normalized X tip displacement for terpolymer bending unimorph.

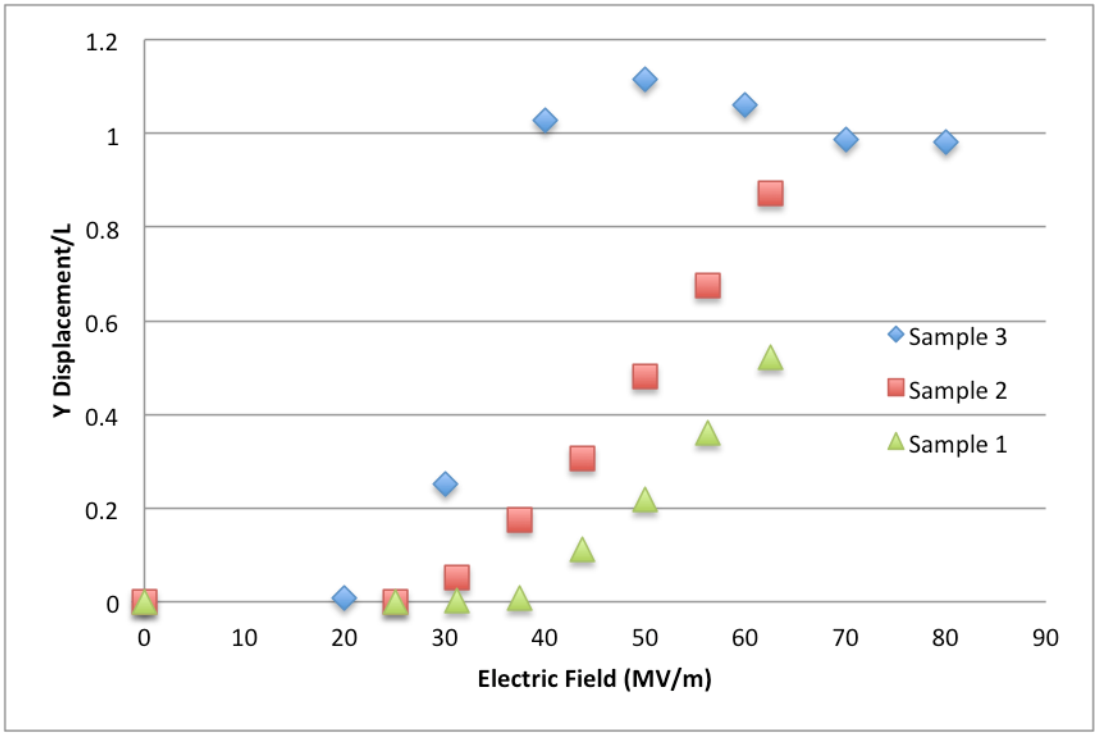

Figure 28: Normalized Y tip displacement of terpolymer bending unimorph.

From these graphs, it can be seen that for all three samples, the actuation of the sample increased as the applied voltage increased. Although the three samples were different lengths, since the displacement values are normalized, it is surprising to see that the three samples did not have very similar displacements to the same applied field. For the tip displacement measurements, sample 1 and 2 both have an increase tip displacement as the field is increased across the entire applied range. Sample three, however, had a max tip displacement around 30 MV/m and then the measurements decreased and plateaued at a normalized ratio of about one. This is due to the sample curling up on itself as discussed Chapter 2. As the sample curled up on itself, the measured tip displacement actually decreased. The X and Y displacements give a better idea of how the sample is actually moving, unlike the total tip displacement. For all three samples, the X displacement exhibits a peak value and then begins to decrease. This shows that

the sample tip moves as far horizontal as it can during the actuation, and at higher fields, the tip actually begins to return, horizontally, to where it started. In looking at the Y displacement, since this value is increasing continuously for samples one and two, it suggests that after the peak X displacement, rather than returning to the center line, the sample is actually actuating further because it is still moving up.

Along with the terpolymer unimorph, bending was explored using a MAE unimorph. This sample consisted of only one strip of 3 cm x 1 cm MAE with no other substrates attached to the active material. Similar to the terpolymer unimorph sample, a video was taken of the sample as the magnetic field applied to the sample was increased. Still images were captured from the video and compiled, as seen in Figure 29. At specified applied magnetic fields, the images were used to measure the sample tip displacement, X tip displacement, and Y tip displacement as seen in Figure 30, Figure 31, and Figure 32 respectively. From these figures, it can be seen that as the magnetic field increases, the tip displacement, X tip displacement, and Y tip displacement all increase as well. Unlike the terpolymer unimorph, these tip displacements show a more linear response to the increase in applied field. Also, since the length of the sample is taken into account by dividing each displacement by the length, it can be observed that the displacements for the MAE are not as large as the displacements for the terpolymer.

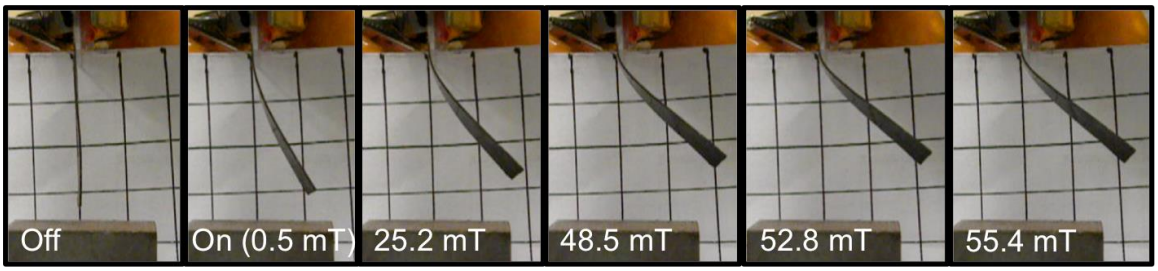

Figure 29: MAE bender sample actuated at different magnetic fields. [4]

[4] Thank you to my lab mate Shreya Trivedi for preparing and testing this MAE bender sample.

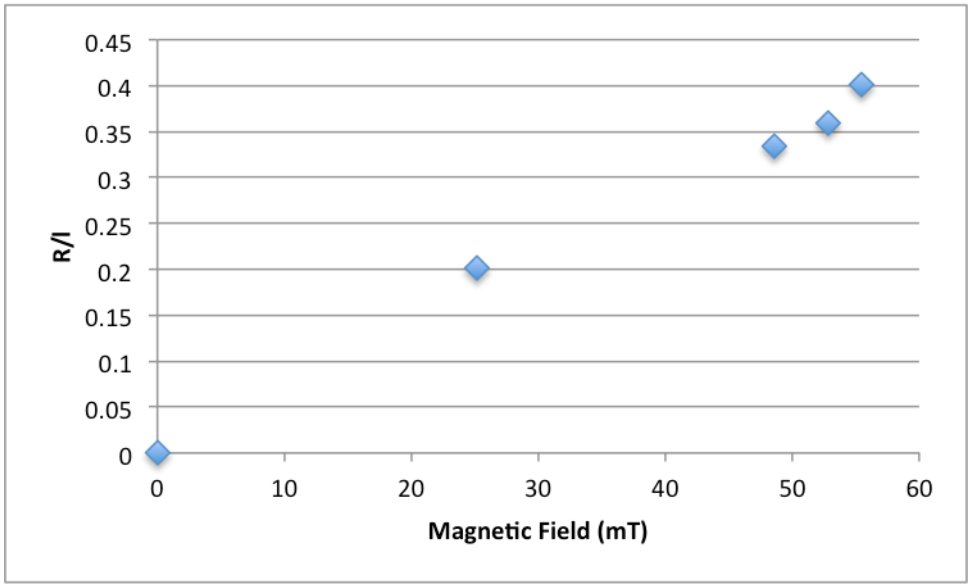

Figure 30: Normalized tip displacement of MAE bending unimorph.

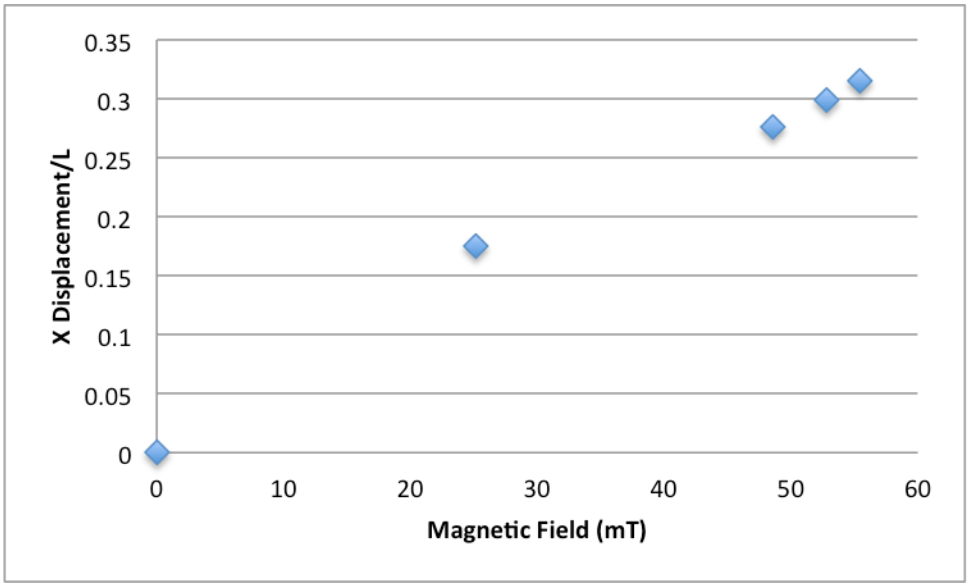

Figure 31: Normalized X tip displacement of MAE bending unimorph.

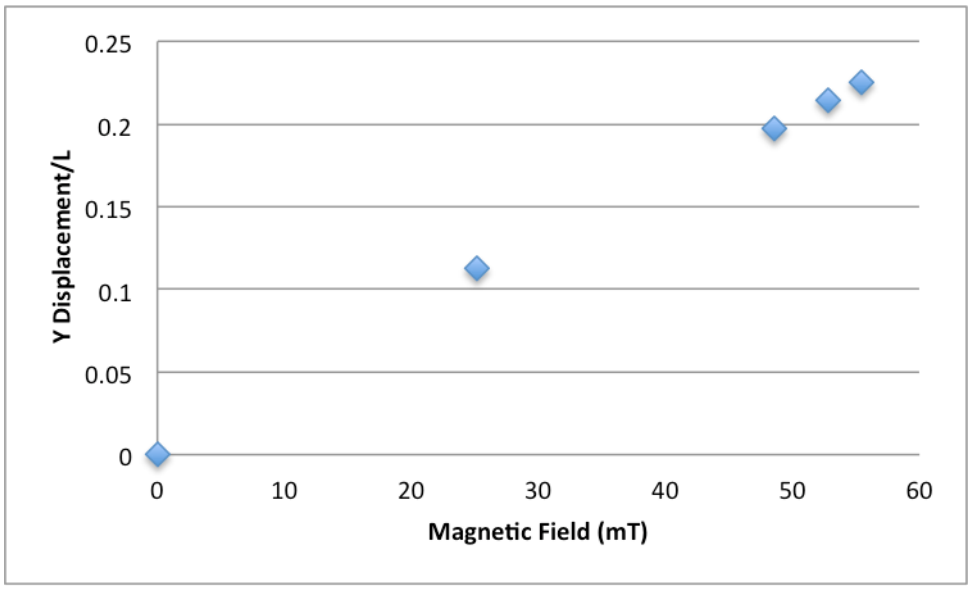

Figure 32: Normalized Y tip displacement of MAE bending unimorph.

From these three figures, (Figure 30, Figure 31, Figure 32), it can be observed that the actuation of the MAE unimorph sample increased as the applied magnetic field increased, as was expected. All three measurements show a linear trend relating magnetic field to displacement, which is different than the terpolymer unimorph that showed non-linear trends relating the actuation to the applied electric field. When looking at the normalized X and Y displacements, it can be seen that the normalized X displacement is slightly greater than the Y displacement which means that the sample tip had more actuation in the vertical direction than in the horizontal direction.

Folding Actuation

Folding was also explored by creating a unimorph using terpolymer as the active material and then adding extra pieces of scotch tape to the unimorph to create a notch in the sample. Parameters that were varied were the notch size and the number of notches. Schematics of the

configurations of samples with one notch and two notches can be seen in Figure 6 (b) and (c) respectively.

The sample dimensions tested with a single notch can be found in Table 5. Again, as discussed in Chapter 2, still images were taken from the video for each sample at each applied electric field. A compilation of the images taken for sample 1 can be found in Figure 33. The applied voltage is shown in these pictures. In order to convert from the applied voltage to the applied electric field, Equation 2 is used. From the still images taken for each sample at each applied electric field, the tip displacement and angle were measured and can be seen in Figure 34 and Figure 35 respectively. The samples show data stopping at different electric fields because some samples failed at lower electric fields than others. From this data, it can be seen that the most actuation was obtained by the sample with the 1 cm notch size.

Table 5: Terpolymer Single Notch Sample Dimensions

Sample	Length (cm)	Width (cm)	Thickness (μm)	Notch Size (cm)
1	6	2	40	1
2	3	1	40	0.5
3	6	2	40	0.5
4	6	2	40	0.1

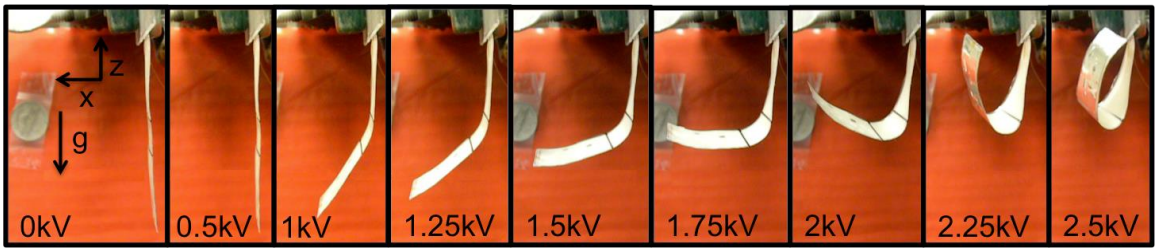

Figure 33: Terpolymer single notch sample 1 actuation at different applied voltages.

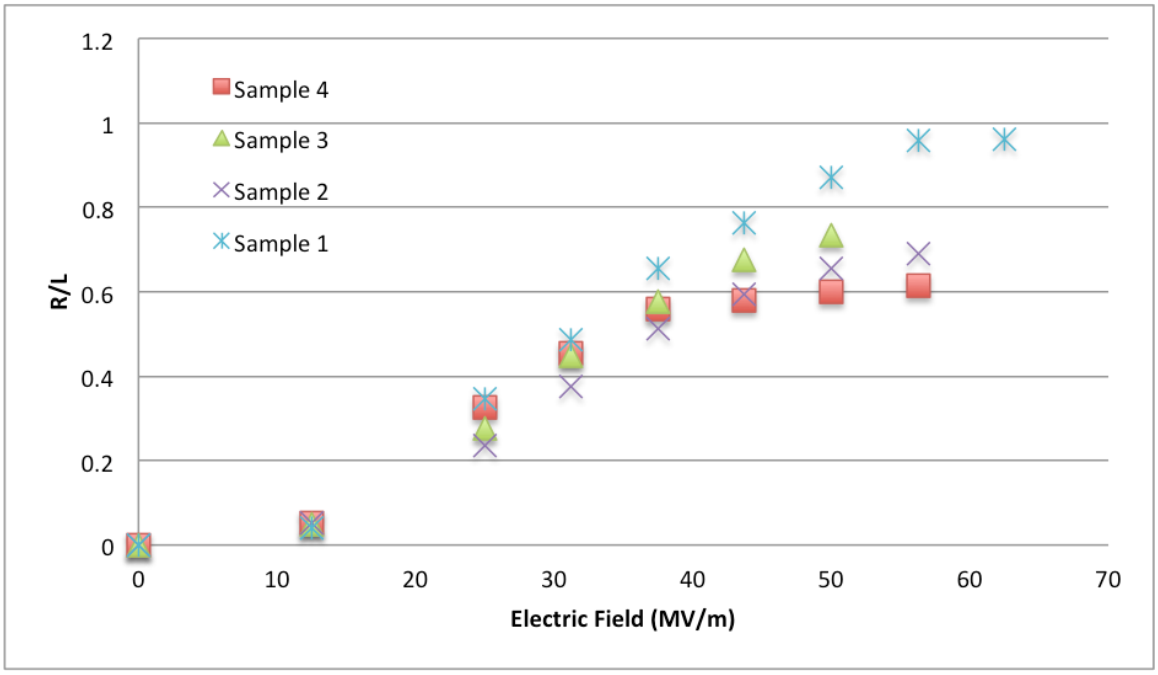

Figure 34: Normalized tip displacement of terpolymer unimorph with a single notch.

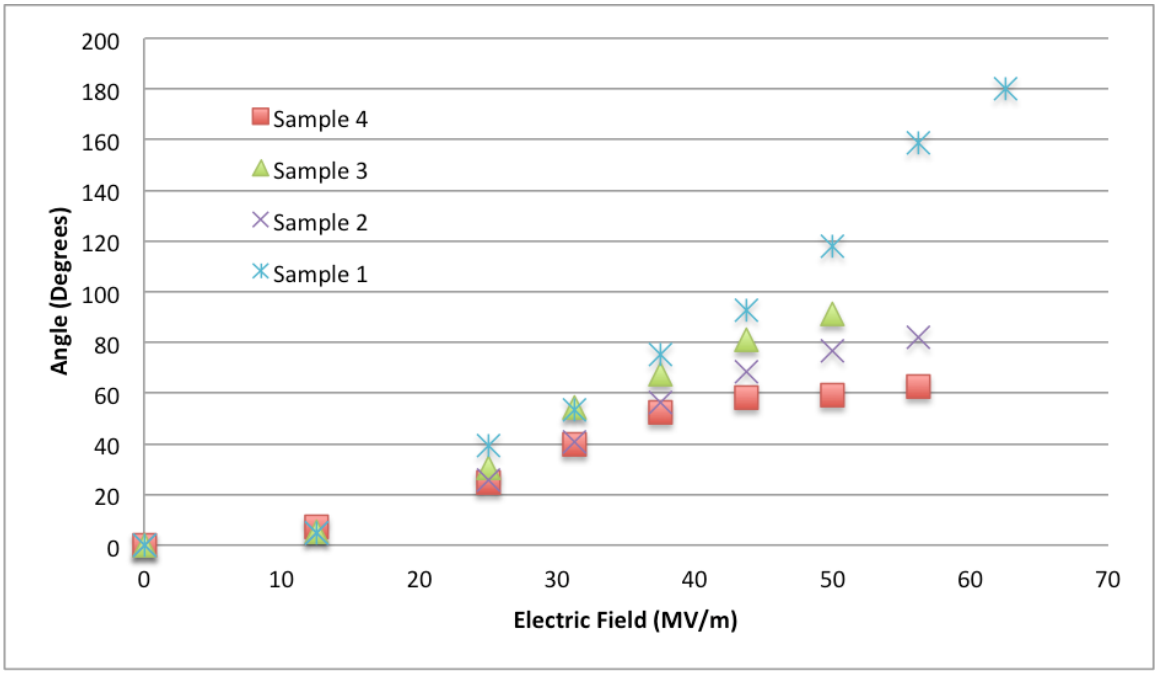

Figure 35: Angle measurements for terpolymer unimorph with a single notch.

By analyzing both the tip displacement and angle measurement, it can be observed that as the applied electric field increased, the actuation of all of the notched samples increased as well. As expected, the measured angle increased as the applied field increased. These samples produced normalized data that were much closer together than that of the bending unimorphs, even though the folding unimorphs had different dimensions. With that being said, the 6 cm x 2cm sample with 1 cm notch did produce the highest angle and tip displacement for every applied field. Over all, the notched strategy to try to create a fold (localized bending) worked really well as can be seen by comparing Figure 25 and Figure 33. By comparing these two compilations of images of both the bender and folder sample at different applied fields, a clear difference in the sample motion can be seen.

Sample dimensions for samples tested with two notches can be found in Table 6. A compilation of the still images taken from the actuation of sample 2 can be seen in Figure 36. As seen in this figure, as the applied field increases, the unimorph clearly folds in the two notch locations. The sample folds so much at both notch locations that the unimorph actually curls up on itself. For example, the images for the sample with an applied voltage of 2 kV looks very similar to the image for the sample under an applied voltage of 2.25 kV. This result is due to the fact that the sample is folded in on itself, causing the sample to be unable to actuate further since it is in contact with itself. Tip displacement for both samples was measured and recorded in Figure 37, but as seen in Figure 36, the samples actually folded in on themselves. This caused the tip displacement to appear to go down at higher applied fields as seen in Figure 37, even though the sample actuation was still increasing. To account for this, the distance the tip traveled was deemed to be a better representation of sample actuation, and therefore it was recorded and plotted in Figure 38. This is a better representation of which sample had more actuation. It can be observed from Figure 36 that the distance traveled for sample 2 was higher than that of sample 1 which correlates with what was actually observed, unlike the trend seen in just the tip

displacement graph. The angles of each sample at each applied field were also measured as discussed in Chapter 2. Figure 39 shows these angle measurements with angle 1 measured at the top notch on the sample and angle 2 measured at the bottom notch of the sample (angle 1 and angle 2 can be seen in Figure 24). From this data, it is again seen that the sample with the 1 cm notch sizes had more actuation than the one with 0.1 cm notch size.

Table 6: Terpolymer Double Notch Sample Dimensions

Sample	Length (cm)	Width (cm)	Thickness (μm)	Notch Size (cm)
1	6	2	38	0.1
2	6	2	38	1

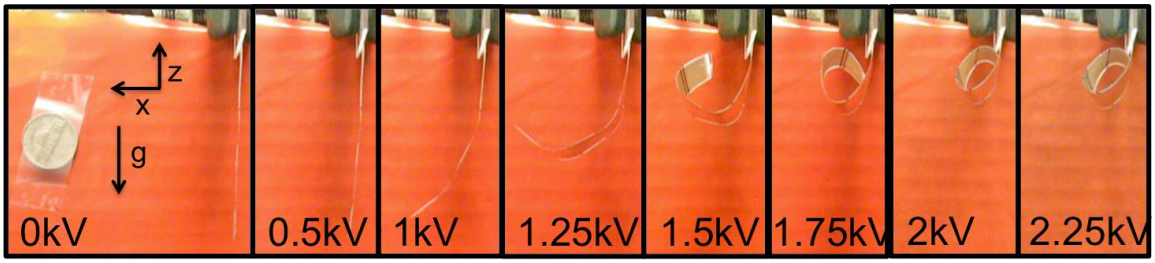

Figure 36: Terpolymer double notch sample 2 actuation at different applied voltages.

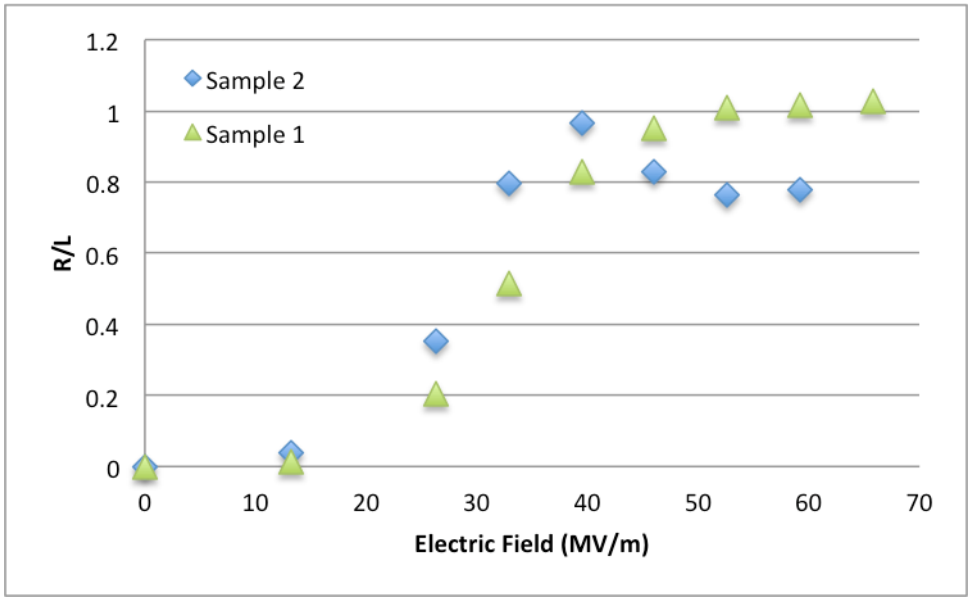

Figure 37: Normalized tip displacement of terpolymer unimorph with double notches.

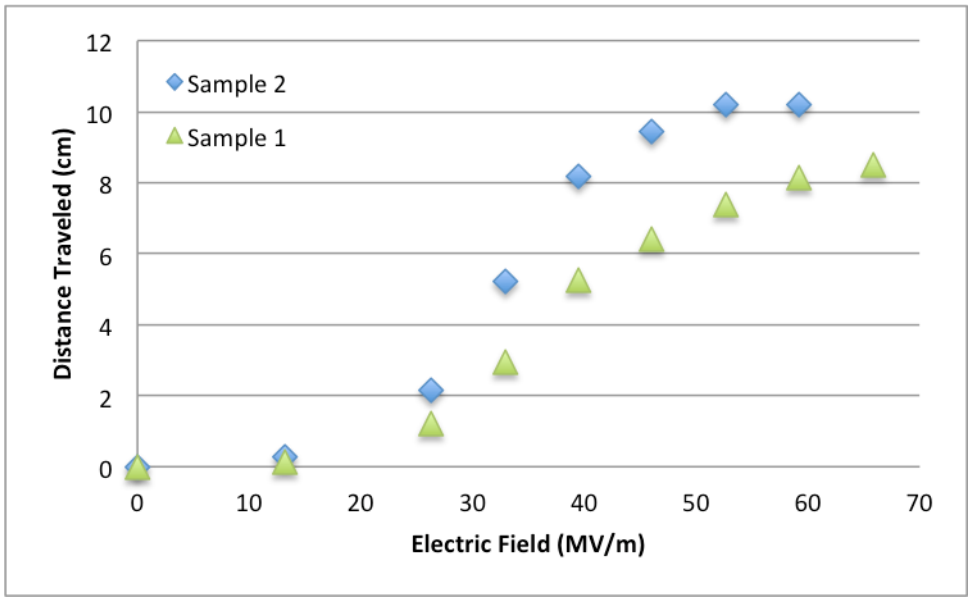

Figure 38: Distance trip traveled of terpolymer unimorph with double notches.

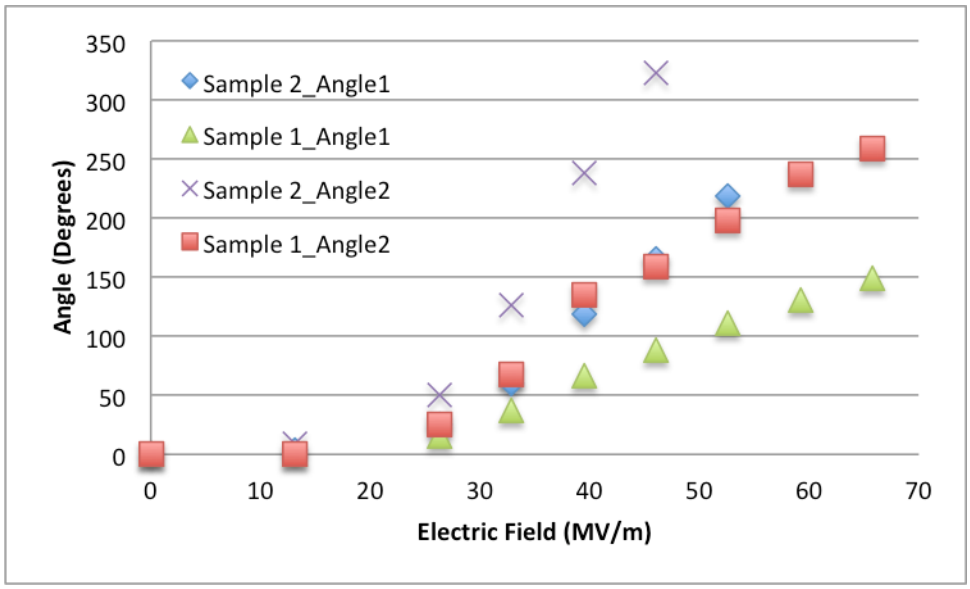

Figure 39: Angle measurements for terpolymer unimorph with double notches.

For both notch sizes, it can be observed form Figure 39 that the second angle on the sample was greater than the first angle for the same applied fields. This could be due to the fact that the second notch has less material that it would have to move (just the bottom section of the sample) in order to actuate where as the first notch has the entire middle section and the end of the sample that it would need to move during actuation. Again, the sample with 1 cm notches showed a higher distance the tip traveled, and greater angles at every applied field. It is also interesting to note that the distance the tip traveled and both the angles show a non-linear response to the applied field.

Multi-field Actuation

After bending and folding were explored using terpolymer and MAE separately, both terpolymer and MAE were combined into one sample configuration to make multi-field actuators (see Figure 9, Chapter 2). The dimensions of the samples were restricted by the space between the

pole faces of the magnets that were used to apply the external magnetic field. Since the gap was smaller than 6 cm, it was decided to make samples that were 3 cm in length. In order to keep the same ratio as the 6 cm x 2 cm samples that showed good actuation in the previous experiments, the multi-field samples were fabricated to be 3 cm x 1 cm samples.

The multi-field samples were first tested in response to an applied electric field and then to a magnetic field generated by the C-magnet. However, as discussed previously, the fields produced by the C-magnet did not provide a wide range of data and the sample moved outside of the pole faces (causing the sample to be affected by a non constant field) during actuations. Because of this, additional samples were fabricated and tested in the horizontal and vertical magnets depending on the type of actuation expected.

The multi-field bender sample actuation in response to an applied electric field can be seen in Figure 40a, and the response to an applied magnetic field (from the horizontal magnet) can be seen in Figure 40b.

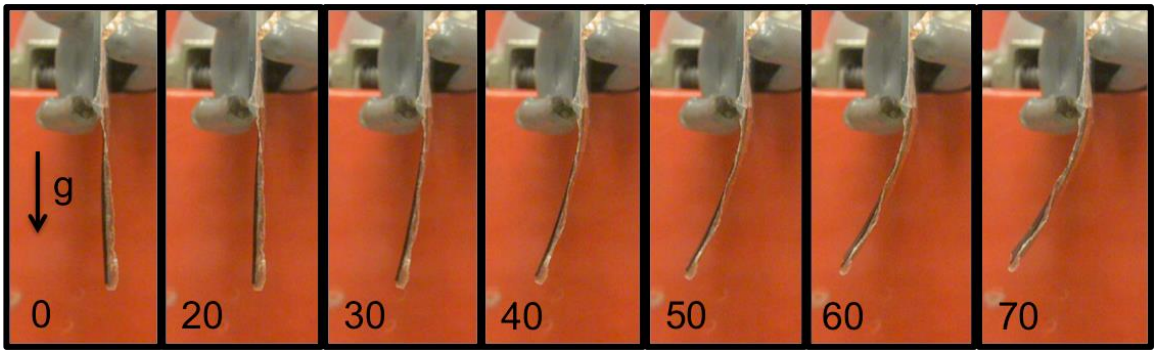

(a)

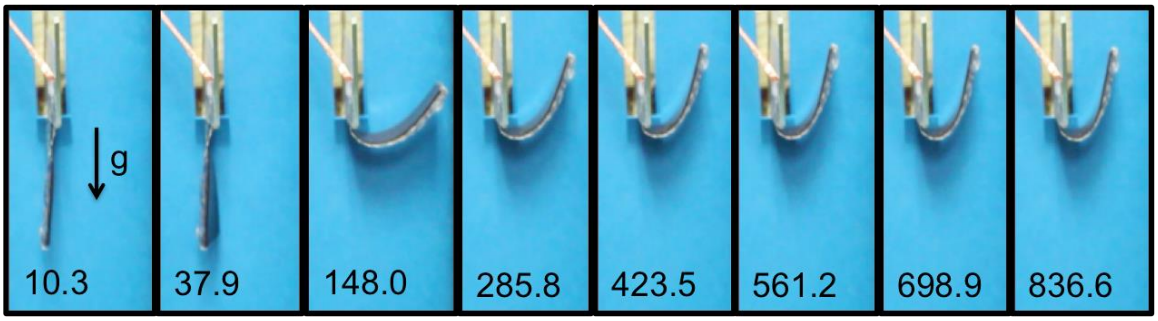

(b)

Figure 40: Multi-field bender sample (a) actuation at different applied electric fields (in MV/m) (b) actuation at different applied magnetic fields (in mT).

The videos taken for each multi-field bender sample at different applied fields (both magnetic and electric) were used to calculate the tip displacement at each applied field as discussed in the Actuation Measurement Details section. Figure 41 and Figure 42 show the measurements taken for both samples in both types of fields; sample 1 was actuated in the C-magnet and sample 2 was actuated in the horizontal magnet.

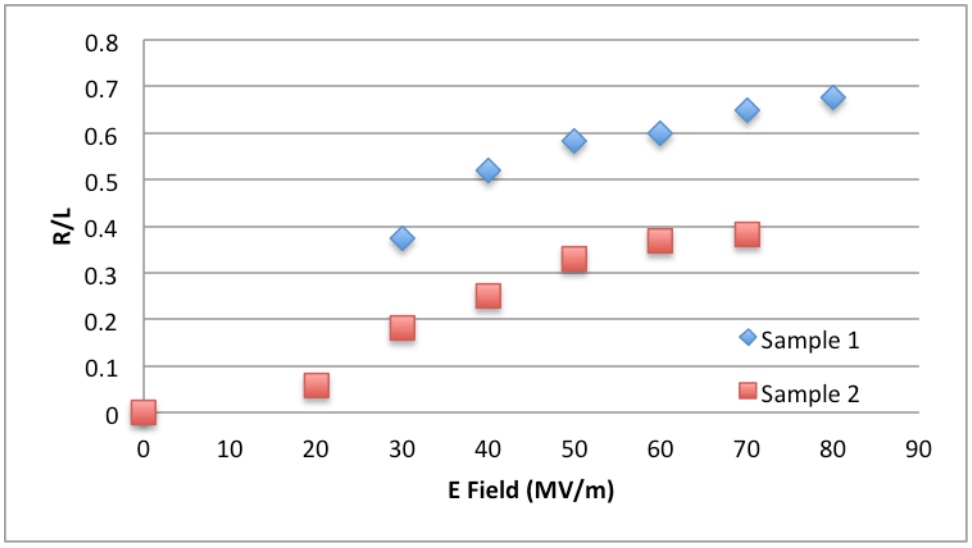

Figure 41: Multi-field bender tip displacement for electrical actuation, where sample 1 was magnetically tested using the C-Magnet and sample 2 was magnetically tested using the horizontal magnet.

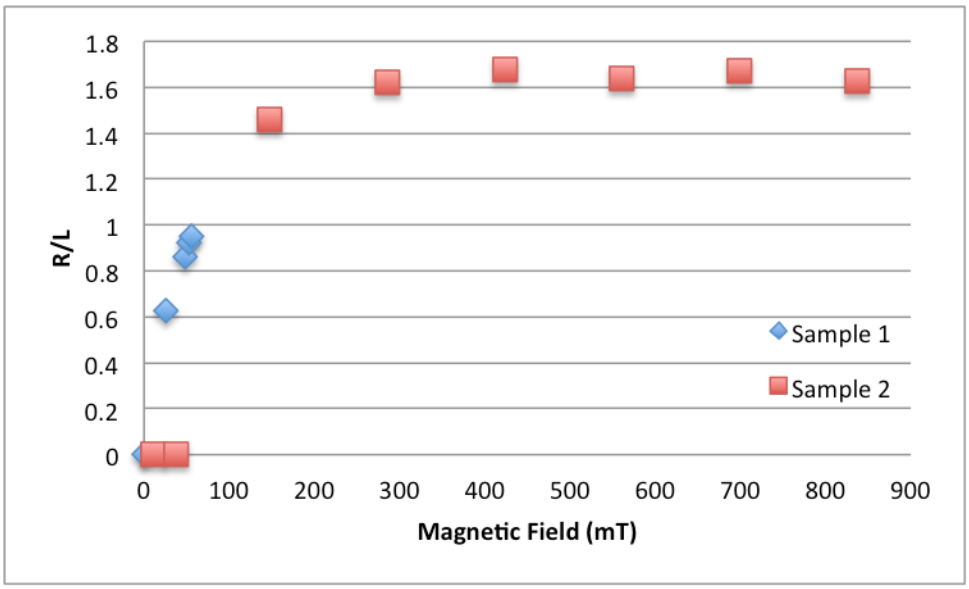

Figure 42: Multi-field bender tip displacement for magnetic actuation, where sample 1 was magnetically tested using the C-Magnet and sample 2 was magnetically tested using the horizontal magnet.

When looking at Figure 41, it is surprising that the samples showed very different normalized tip displacements. The main thing that was different about sample 1 and sample 2 was where each sample was magnetically actuated which should not have an effect on the electrical actuation of the sample. Since the samples had the same dimensions, it was unexpected that the tip displacements from the same applied electric fields would be so different. As far as the magnetic field, there was expected to be a big difference between sample 1 and sample 2, as seen in Figure 42. From this figure, you can see how using the horizontal magnet for actuation greatly increased the range of magnetic fields that could be applied to the sample. In comparing the normalized tip displacements for the electric actuation vs. the magnetic actuation, it can be observed that both samples produced more max actuation from the applied magnetic field than the applied electric field.

The multi-field folder sample dimensions was also restricted by the space available between the two pole faces of the magnets used to apply the external magnetic field. Because of

this, the sample length was limited to a size of 3cm. From the earlier folder experiments with just terpolymer, it was observed that the best actuation was achieved from the sample that had dimensions of 6 cm x 2 cm with a 1cm notch. In order to keep the ratio the same, the multi-field sample was made with dimensions of 3 cm x 1 cm with a 0.5 cm notch. This notch was created used the two patched of MAE as seen in Figure 9 (b). Folding was obtained when applying a magnetic field by flipping the pole directions of the MAE patches as seen in Figure 9 (b). The compilation of still images taken from applying different electric fields can be seen in Figure 43a. The compilation of still images taken from applying different magnetic fields (using the vertical magnet) can be seen in Figure 43b.

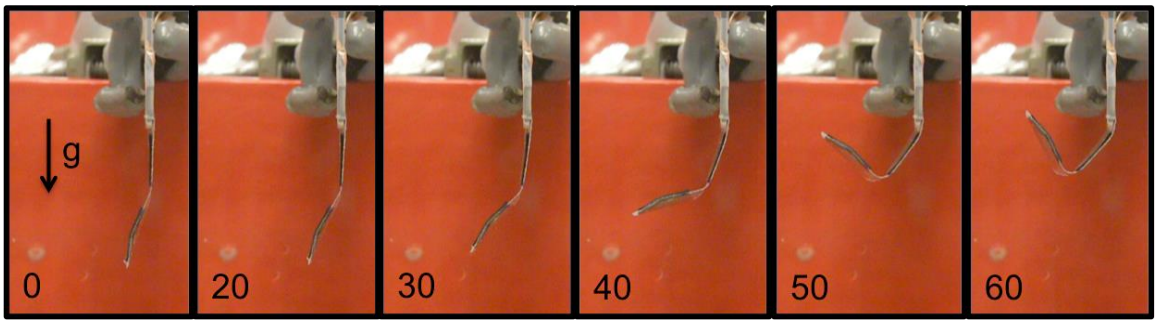

(a)

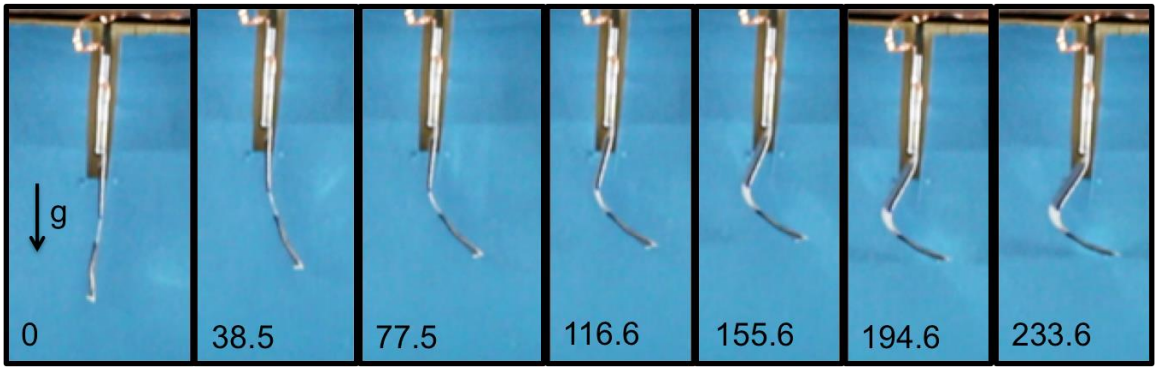

(b)

Figure 43: Multi-field folder sample (a) actuation at different applied electric fields (in MV/m), (b) actuation at different applied magnetic fields (in mT).

From these images, the sample tip displacement and the sample angle were measured as at each applied field as explained previously. Data was collected for both the sample that was tested using the C-magnet (sample 1) as well as the sample that was tested using the vertical magnet (sample 2). The tip displacement data for both the electric and magnetic actuation can be seen in Figure 44 and Figure 45 respectively. The angle measurements recorded can be seen in Figure 46 and Figure 47 respectively.

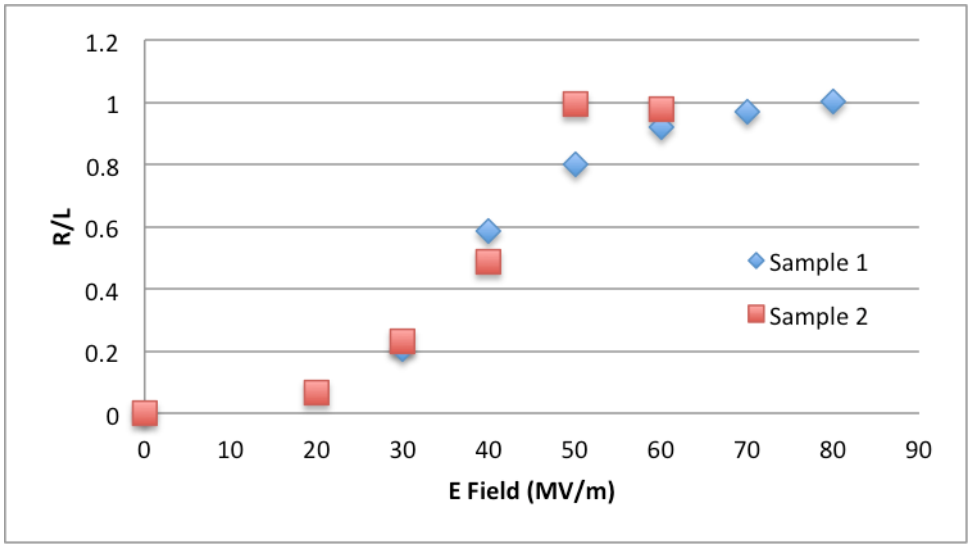

Figure 44: Multi-field folder tip displacement for electrical actuation, where sample 1 was magnetically tested using the C-Magnet and sample 2 was magnetically tested using the vertical magnet.

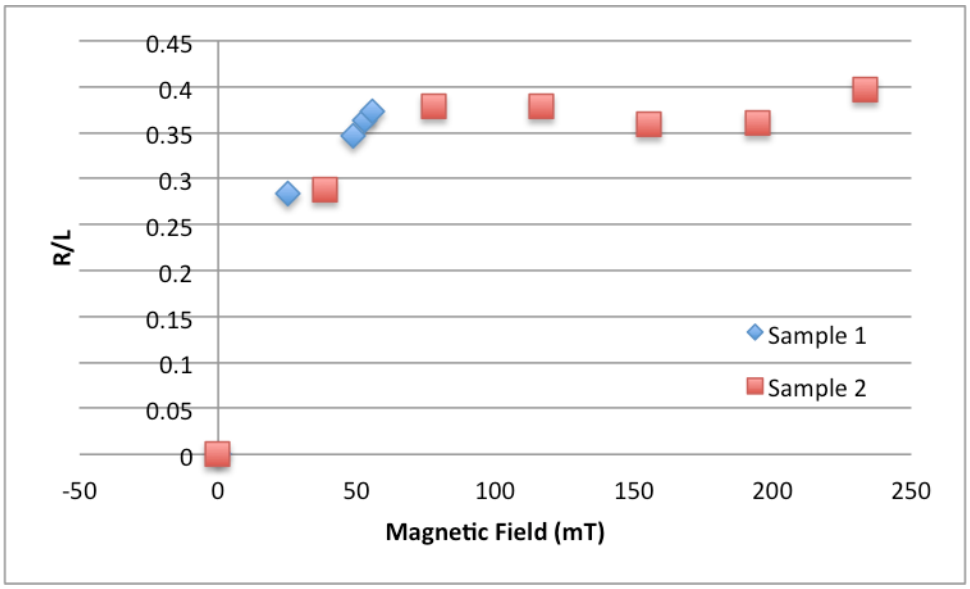

Figure 45: Multi-field folder tip displacement for magnetic actuation, where sample 1 was magnetically tested using the C-Magnet and sample 2 was magnetically tested using the horizontal magnet.

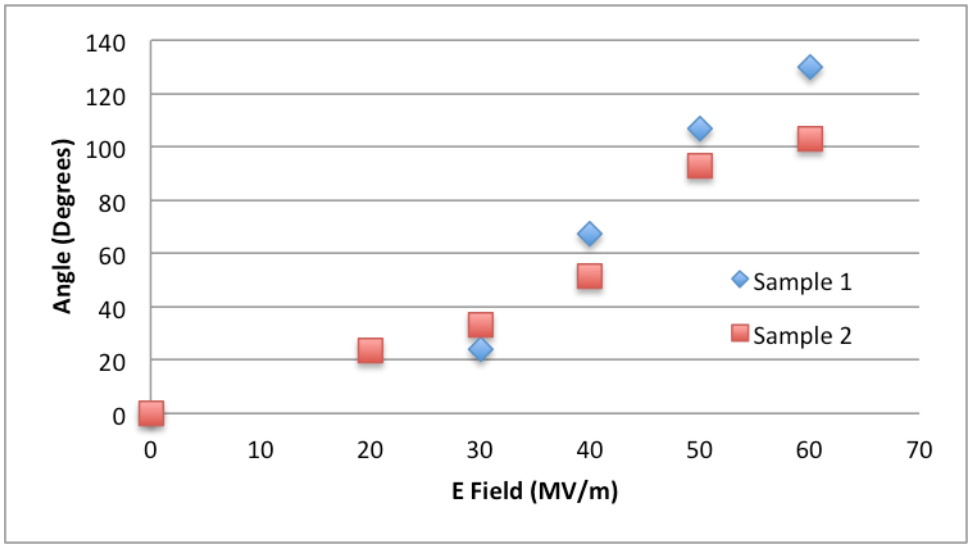

Figure 46: Multi-field folder angle measurement for electric actuation, where sample 1 was magnetically tested using the C-Magnet and sample 2 was magnetically tested using the horizontal magnet.

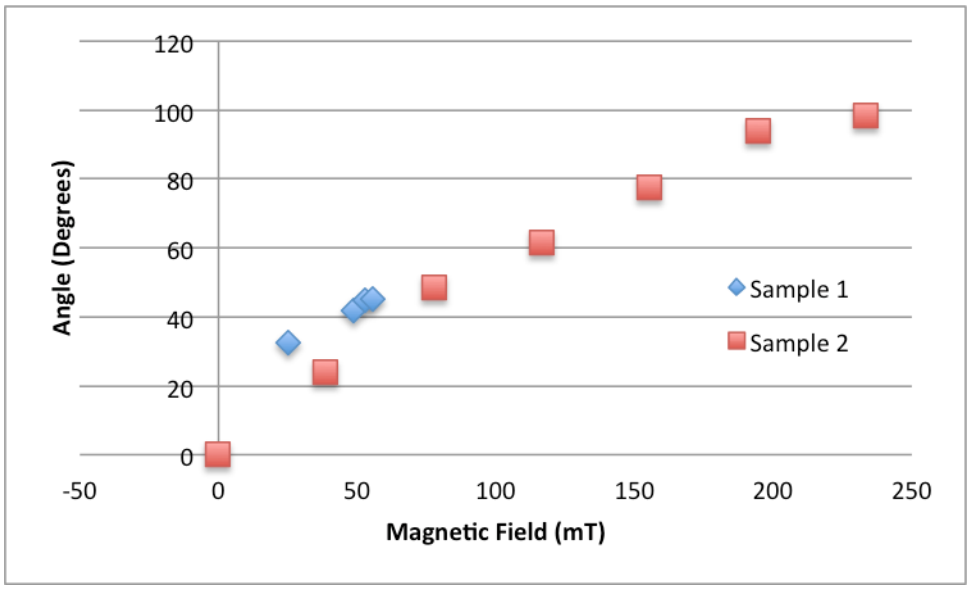

Figure 47 Multi-field folder angle measurement for magnetic actuation, where sample 1 was magnetically tested using the C-Magnet and sample 2 was magnetically tested using the horizontal magnet.

From Figure 44, it can be seen that both multi-field folder samples produced similar tip displacements when under the applied electric field. This is expected because, similar to the multi-field bending samples, the main difference between sample 1 and sample 2 was which magnet was used to apply the magnetic field to the sample, which should not effect the electric field testing since the fields were not applied simultaneously. Similarly, as seen in Figure 46, both sample 1 and sample 2 produced similar angles from the same applied electric field. On the other hand, looking at Figure 45 and Figure 47, a big difference can be seen between sample 1 and sample 2 for the magnetic actuation. It can be seen that for both tip displacement and angle, the vertical magnet allowed for a much bigger test range in the magnetic fields applied to the sample. It can also be seen that, although sample 1 has few points, the points from the sample tested in the C-magnet are very close to those of the sample tested in the vertical magnet. This is a good thing because, no matter what is producing the magnetic field, it would be expected that the samples produce similar actuation at similar applied fields since the MAE patches used on both were the same wt% and same thickness.

Chapter 4 Conclusion and Future Work

Conclusion

Throughout this research, many different experiments were performed which lead to successfully fabricating a multi-field actuation configuration that responded to both electric and magnetic fields. First, bending actuation of a terpolymer unimorph was successfully demonstrated. A curvature over the entire sample was seen, and higher tip displacement was observed as greater electric fields were applied. Bending actuation was also successfully demonstrated in a unimorph sample of MAE. With higher applied magnetic fields, higher sample tip displacement was observed.

Next, folding was successfully demonstrated for a terpolymer unimorph with both single and double notch configurations. Single notch folding was demonstrated using terpolymer samples of varying dimensions and notch sizes. It was observed that the 6 cm x 2 cm sample with a notch size of 1 cm produced the highest actuation, as measured by tip displacement and folding angle compared to other samples at the same applied electric field. This sample configuration and geometry were used later in the project to fix the dimensions of the multi-field folder sample. Double notch folding was explored next using terpolymer unimorphs with different notch dimensions. This set of experiments showed that a different type of overall motion could be obtained from the sample when high electric fields are applied and two distinct notches are present; specifically, at high electric fields, the sample with double notches curled in on itself, to the point where additional actuation could not be produced because the sample was hitting itself. As in the bender case, the sample with dimensions 6 cm x 2 cm with 1 cm notches showed higher folding actuation at all applied electric fields.

Lastly, multi-field samples were successfully actuated in both an electric field as well as a magnetic field. It was shown that one sample comprised of a layer of terpolymer and a layer of MAE could produce bending in one direction when an electric field was applied and bending in the opposite direction when placed in a magnetic field. This showed that it was possible to create one sample that would respond to both electric and magnetic fields. By changing the sample configuration and adding a notch on the MAE side, multi-field folding was successfully achieved. When the electric field was applied, the sample folded in one direction and folded in the other direction when placed in the magnetic field. Actuation of the sample at higher magnetic fields (produced by the vertical and horizontal magnets) produced greater tip displacement and angle measurements for each sample. In summary, multi-field bending and folding were successfully demonstrated. This successful demonstration is beneficial to the field because there is not a lot of work preformed used multi-field actuators. There has been previous modeling done to predict the motion of multi-field actuators, but since this is still a new concept, this thesis showing the proof of concept of multi-field actuators is a step in the right direction for furthering this field. Using this better understanding of multi-field configurations along with both bending and folding, more complex designs of structures will be able to be explored. Also, by showing successful multi-field actuation, this could lead to structures that are multi-functional; providing one function when actuated in an electric field and serving a different function when actuated in a magnetic field. Overall, the successful actuation of multi-field samples is a beneficial finding and demonstration.

Future Work

The next step to further this research area and understanding would be to repeat the experiments preformed to ensure repeatability of all results. The experimental work performed throughout this project will be used to validate modeling efforts by collaborators. It would also be

beneficial to explore double notch multi-field actuator samples that would have two distinct notches in the sample, similar to the double notch terpolymer samples tested in this project. Double notch multi-field actuator samples were not researched in this project because it was decided that the sample size restrictions (max 3 cm length) needed to fit into the C magnet for magnetic actuation would not leave enough room on the sample to have two distinct notches. Moving forward, this is less of an issue because the bigger magnets (horizontal and vertical magnets) used at the end of the experimental process both have a greater gap between the two pole faces, which would allow for a longer sample to be tested in the applied magnetic field. Another test that could be performed is to apply one field, such as an electric field, and then apply a second field, such as a magnetic field, while holding the first field constant. Here, how the sample responds while both fields are applied at the same time could be observed. Along with these configurations, more complex structures could be investigated. For example, a multi-field structure that could bend in one section and fold in another would be interesting to explore. Over all, there are an abundance of different directions where this research could lead.

Appendix A

Magnetic Calibrations

Calibration measurements were taken for each magnet using a Gauss meter as described in Chapter 2. The measured data was then plotted, comparing the current output of the power supply and the produced magnetic field measured using the Gauss meter. From these plots, a linear trend line was added and the equation of that line was used throughout the rest of the project to convert the applied current to the magnetic field produced. For the C-magnet, the data was split up between 0-5 amps and 5-14 amps in order to produce trend lines that fit the data better.

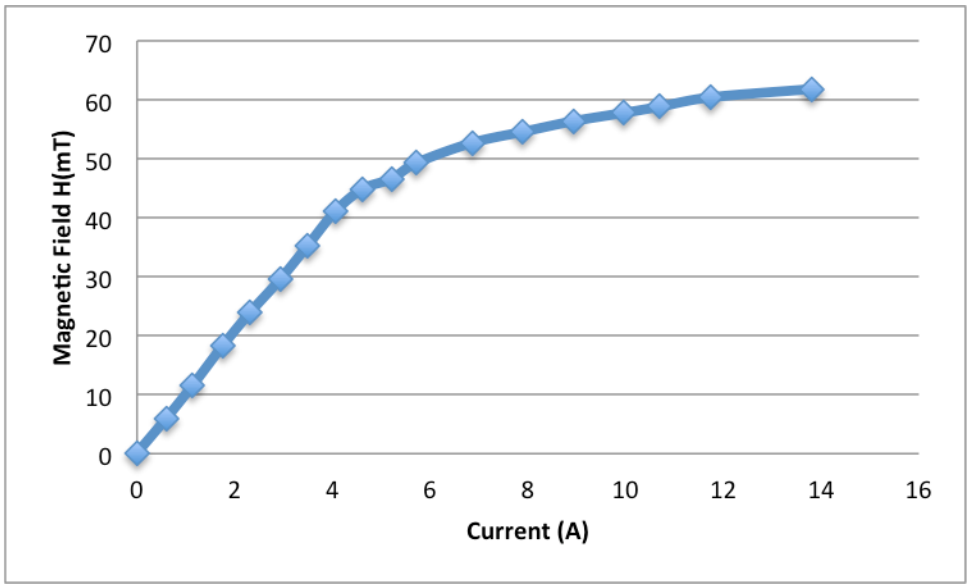

Figure 48: Magnetic field measured using Gauss meter at different applied currents for the C-Magnet

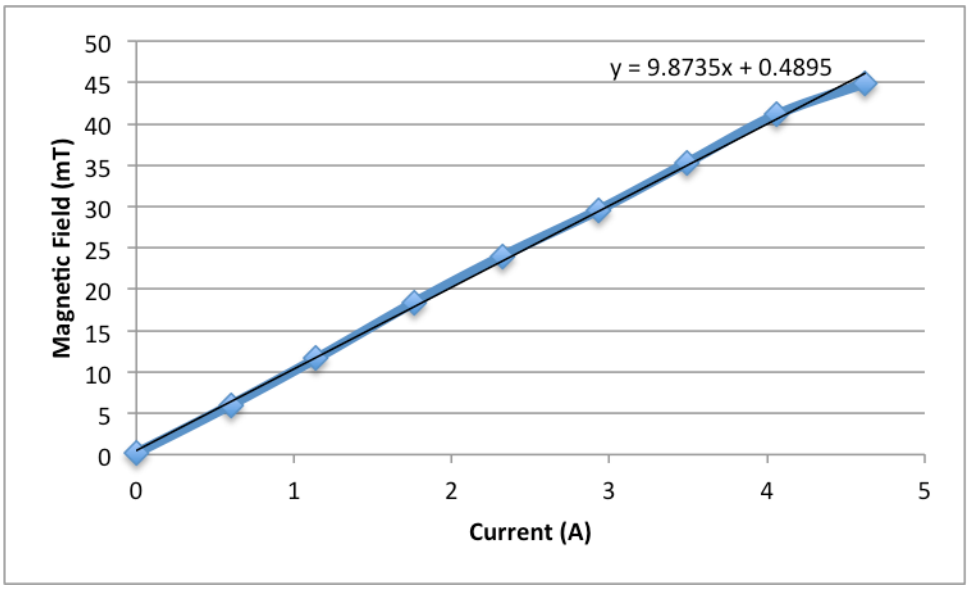

Figure 49: Magnetic field measurements using Gauss meter from 0-5 A for the C-Magnet

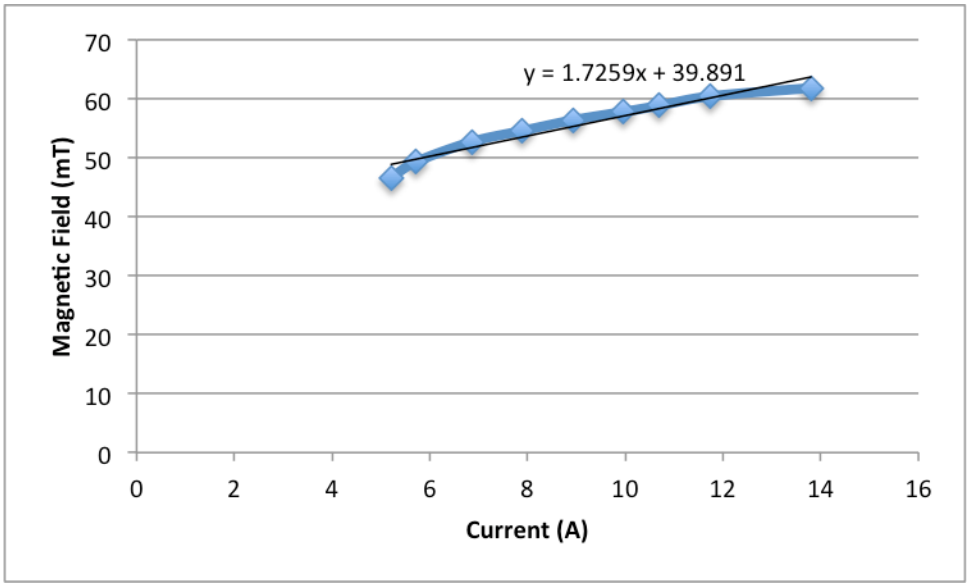

Figure 50: Magnetic field measurements using Gauss meter from 5-14 A for the C-Magnet

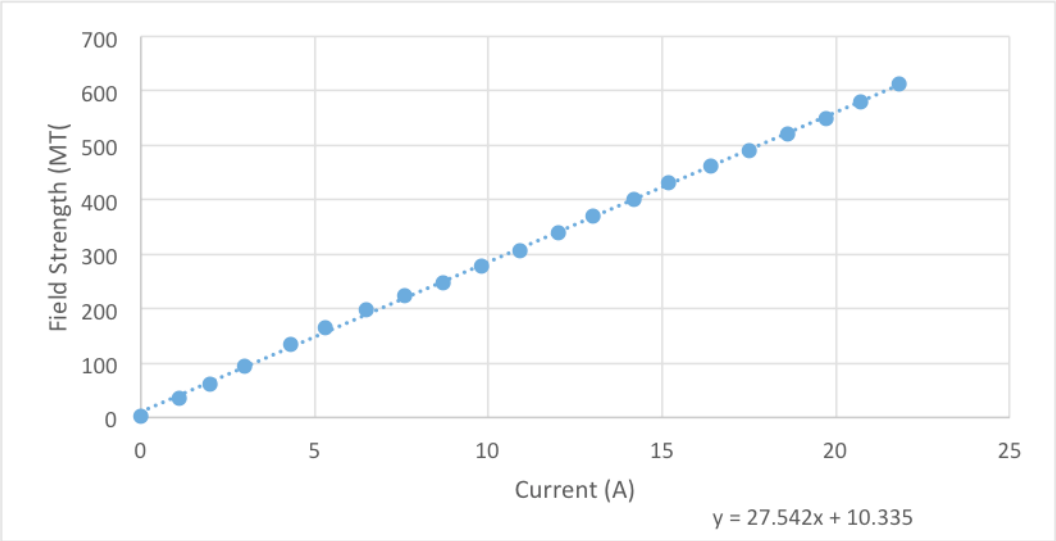

Figure 51: Magnetic field measured using Gauss meter at different applied currents for the Horizontal magnet. [5]

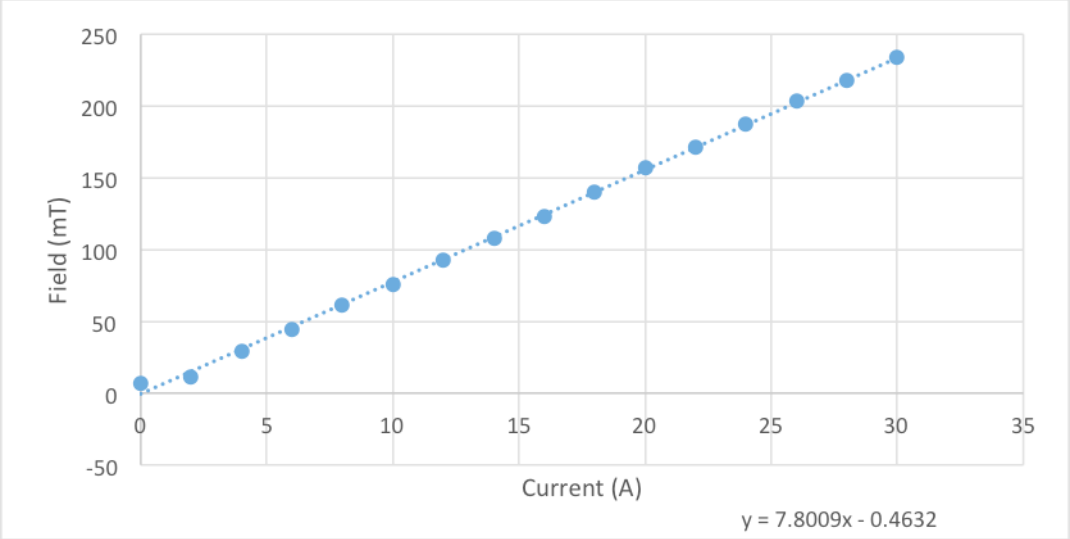

Figure 52: Magnetic field measured using Gauss meter at different applied currents for the Vertical magnet.[5]

[5] Thank you to my lab mate Corey Breznack for providing the calibration data.

Works Cited

[1] Robert J. Lang, "Origami Design Secrets: Mathematical Methods for an Ancient Art," *The Mathematical Intelligencer*, vol. 27, no. 2, pp. 92-95, 2005.

[2] Robert J. Lang, "Origami: Complexity Increasing," *Engineering and Science*, pp. 16-23, Winter 1989.

[3] S Ahmed, Z Ounaies, and M Frecker, "Investigating the performance and properties of dielectric elastomer actuators as a potential means to actuate origami structures," *Smart Materials and Structures*, vol. 23, no. 9, August 2014.

[4] Kaori Kuribayashi et al., "Self-deployable origami stent grafts a s a biomedical application of Ni-rich TiNi shape memory alloy foil," *Materials Science and Engineering:A*, vol. 419, no. 1-2, pp. 131-137, March 2006.

[5] Shannon A. Zirbel et al., "Accommodating Thickness in Origami-Based Deployable Arrays," *Journal of Mechanical Design*, vol. 135, no. 11, Oct 2013.

[6] Samuel M. Felton et al., "Self-folding with shape memory composites," *Soft Matter*, vol. 9, pp. 7688-7694, June 2013.

[7] Jennie Ryu et al., "Photo-origami-Bending and folding polymers with light," *Applied Physics Letters*, vol. 100, April 2012.

[8] Saad Ahmed et al., "Multi-field Responsive Origami Structures: Preliminary Modeling and Experiments," in *IDETC/CIE*, Portland, 2013.

[9] Saad Ahmed, Erika Arrojado, Nirmal Sigamani, and Zoubeida Ounaies, "Electric field responsive origami structures using electrostriction-based active matierals," *Proc. of SPIE*, vol. 9432, 2015.

[10] Yuhuan Xu, *Ferroelectric Materials and Their Applications*.: North-Holland, 1991.

[11] Francois Bauer, Qiming Zhang, and Eric Fousson, "Ferroelectric Relaxor Terpolymers: Properties and Potential Applications," in *Applications of ferroelectrics, 2006. isaf '06. 15th ieee international symposium*, Sunset Beach, NC, 2006, pp. 114-119.

[12] Baojin Chu et al., "A Dielectric Polymer with High Electric Engergy Density and Fast Discharge Speed," *Science*, vol. 313, no. 5785, pp. 334-336, July 2006.

[13] Hari Singh Nalwa, *Ferroelectric Polymers Chemistry, Physics, and Applications*, Ltd. Hitachi, Ed.: Marcel Dekker, Inc., 1995.

[14] Francois Bauer, Jean Fabien Capsal, Quentin Larcher, and F. Domingues Dos Santos, "Advances in relaxor ferroelectric terpolymer: New applicaitons," in *Applications of Ferroelectrics (ISAF/PFM), 2011 International Symposium on Piezoresponse Force Microscopy and Nanoscale Phenomena in Polar Materials*, Vancouver, BC, 2011, pp. 1-4.

[15] Francois Bauer, "Relaxor fluorinated polymers: novel applications and recent debelopments," *IEEE Transactions on Dielectrics and Electrical Insulation*, vol. 17, no. 4, pp. 1106-1112, August 2010.

[16] Philip Shepherd, Kajal K. Mallick, and Roger J. Green, "Magnetic and structural properties of M-type barium hexaferrite prepared by co-precipitation," *Journal of Magnetism and Magnetic Materials*, no. 311, pp. 683-692, 2007.

17] R. H. Victora, "Micromagnetic predictions for barium ferrite particles," *Journal of Applied Physics*, vol. 63, no. 3423, 1988.

18] Darja Lisjak and Simona Ovtar, "The Alignment of Barium Ferrite Nanoparticles from Their Suspensions in Electric and Magnetic Fields," *The Journal of Physical Chemistry*, vol. 117, pp. 1644-1650, 2013.

19] Jeong-Hoi Koo, Alexander Dawson, and Hyung-Jo Jung, "Characterization of actuation properties of magnetorheological elastomers with embedded hard magnetic particles," *Journal of Intelligent Material Systems and Structures*, vol. 23, no. 9, pp. 1049-1054, June 2012.

20] Paris von Lockette and Robert Sheridan, "Folding actuation and locomotion of novel magneto-active elastomer (MAE) composites," in *SMASIS*, Snowbird, UT, 2013.

21] Xiaojing Jing, Xiangqian Shen, Haojie Song, and Fuzhan Song, "Magnetic and dielectric properties of barium ferrite fibers/poly(vinylidene fluoride) composite films," *Springer Science+Business Media B.V.* , April 2011.

22] Y.D. Zhang and J. I. Budnick, "Dynamic alignment of magnetic materials," *Applied Physics Letters*, vol. 70, no. 1083, 1997.

23] P von Lockette et al., "Investigating new symmetry classes in magnetorheological elastomers: cantilever bending behavior," *Smart Materials and Structures*, vol. 20, no. 10, September 2011.

24] Nirmal Shankar Sigamani, Saad Ahmed, and Zoubeida Ounaies, "Effect of processing conditions on the microstrucure and electromechanical response of PVDF FRFE CTFE Terpolymers," in *ASME SMASIS*, Newport, Rhode Island, 2014.

25] Eric W. Wilcox, Spencer Magleby, and Larry L. Howell, "Exploring Movements and Potential Actuation in Action Origami," in *ASME International Design Engineering Teachnical Conference and Computers and Information in Engineering Conference*, 2014.

Academic Vita
Sarah R. Masters

srm311@psu.edu

EDUCATION

Bachelor of Science in Engineering Science (Honors)
The Pennsylvania State University, University Park, PA
Schreyer Honors College
Dean's List: All semesters
Graduation: May 2016

RESEARCH EXPERIENCE

NSF-Funded Undergraduate Researcher 2014-15
Active Origami Research Experience and Mentoring (REM)
The Pennsylvania State University, University Park, PA
- Created multi-field actuator using terpolymer and magneto-active elastomer under the direction of Dr. Zoubeida Ounaies
- Coordinated and instructed K-12 engineering outreach

Undergraduate Student Researcher 2013-14
Penn State Applied Research Laboratory, University Park, PA
- Engaged in limited distribution interdisciplinary research
- Collaborated with other undergraduate students

NSF-Funded Undergraduate Researcher Summer 2013
Surface Thin Film Research Experience for Undergraduates (REU)
University of Virginia, Charlottesville, VA
- Engaged in interdisciplinary research under the direction of Dr. Opila
- Designed experiment to observe boria loss in borosilicate glasses
- Created borosilicate glass layer by oxidizing zirconium diboride at high temperatures

LEADERSHIP

Mentor & Leadership Team Member 2013-16
Penn State Women in Engineering Program Orientation (WEPO)
- Provide academic resources to first-year women engineering students
- Set an academic example for peers to optimize retention of 180+ women
- Actively engage in WEP initiatives throughout the academic year

Mentor, PSU Engineering Orientation Networking (EON) 2013-14
Physics Facilitator, Penn State Women in Engineering Program 2013-15

INVOLVEMENT

Treasurer, Society of Engineering Science (SES) 2012-15
Leader, Penn State WEP Girl Scout Saturday Outreach 2013-14
Member, Society of Women Engineers (SWE) 2013-16
Volunteer, Centre County Special Olympics 2009-14

HONORS

SMART Program Participant **2014-18**
Dr. John T. and Carolyn O. Frasier Merit Award 2015
Evan Pugh Scholar (Senior) Award (Top 0.5% of class) 2015
Tau Beta Pi (Engineering Honor Society) 2015-16
The Robert and Myrtle Vierck Scholarship 2014
Kearns/McNitt Award 2014
National Society of Collegiate Scholars 2013-14
Phi Eta Sigma (Freshman Honor Society) 2013-14
Lyle W. and Virginia C. Coffey Scholarship in ESM 2013
Girl Scouts of America Gold Award 2011